TECHNICAL MEMORANDUM

628

Assessment of the Real-Time Fire Emissions (GFASv0) by MACC

Angelika Heil[(1)], Johannes W. Kaiser[(2)], Guido R. van der Werf[(3)], Martin J. Wooster[(4)], Martin G. Schultz[(1)], Hugo Dernier van der Gon[(5)]

(1) Forschungszentrum Jülich, Germany
(2) ECMWF, United Kingdom
(3) VU University Amsterdam, Netherlands
(4) Kings College London, United Kingdom
(5) TNO, Apeldoorn, The Netherlands

July 2010

European Centre for Medium-Range Weather Forecasts
Europäisches Zentrum für mittelfristige Wettervorhersage
Centre européen pour les prévisions météorologiques à moyen

Series: ECMWF Technical Memoranda

A full list of ECMWF Publications can be found on our web site under:
http://www.ecmwf.int/publications/

Contact: library@ecmwf.int

European Centre for Medium Range Weather Forecasts
Shinfield Park, Reading, Berkshire RG2 9AX, England

Abstract

The Global Fire Assimilation System (GFAS) used in MACC provides real-time fire emissions for atmospheric forecasts using satellite-observed fire radiative power (FRP) information from MODIS and SEVERI, which are scaled with a previously published global conversion factor to derive estimates of the dry matter burned. In this report, we evaluate the quality of FRP-based estimates of combustion rates by comparing them with corresponding data from the latest version of the GFED inventory (GFED3). The comparison is done on a global, regional and ecosystem level using annually averaged and monthly data covering the period 2003 to 2009. In general, FRP-based estimates and GFED3 agree well with each other in terms of the temporal variability and the regions of major burning. On a global scale around 80% of the monthly variation in the amount of dry matter burned (GFED3 inventory) can be explained by monthly variations in MODIS FRP. However, GFED3 burned dry matter is on average 2.2 times higher. The difference is most pronounced in areas with potential soil organic matter burning (tropical peat areas and boreal forests with dense humus layer), pointing to limitations in the detection capability of FRP-based approaches in these biomes. We find good correlations of the FRP-based and GFED combustions rates within each of the eight investigated land cover types, though. Therefore, using land cover-specific conversion factors will generally allow reproducing the GFED combustions rates with FRP observations within GFED's estimated accuracy. The remaining major difference is that the MODIS FRP observations appear to detect more fires than are included in GFED. This leads to fire emission distributions that are less localised in time and space. The origin of this difference is not clear and further investigations are needed to decide which distribution is more realistic. We also compare global total monthly CO emissions that have been produced by the MACC real time service (GFASv0) in 2009 to the GFED inventory. Both agree relatively well in terms of total amounts, but there are differences in the seasonal cycles in various regions. The most distinctive difference results from anomalies in the FRP observations by SEVIRI over South America. Others result from gas flaring and the variation of fire types within individual grid cells. Several recommendations for the future development of the GFAS MACC system are derived from the comparisons. We conclude that their implementation will finally result in a fire estimation system that combines the advantages of the well established GFED inventory with those of the new FRP-based approach. As next steps, anomalous SEVIRI observations over South America should be masked out, fuel-type specific conversion factors of FRP into dry matter burned should be implemented, and gas flaring should be masked.

Table of Content

1 Introduction

The MACC project (http://gmes-atmosphere.eu) produces regular forecasts of atmospheric chemical composition and a comprehensive reanalysis covering the period since 2003. A large part of the variability of atmospheric trace constituent concentrations (such as absorbing aerosol, carbon monoxide, hydrogen cyanide and others) is caused by emissions from the combustion of plant matter. Accurate estimates of biomass burning emission of various species are therefore needed in the MACC project for use as boundary condition in the atmospheric analyses and forecasts. Fire emission estimates are calculated in real time with the Global Fire Assimilation System (GFAS) developed within GEMS and MACC. It assimilates satellite-based observations of the fire radiative power (FRP) of the actual fires. The first version, GFASv0, provides data from October 2008 to the present (Kaiser et al. 2009a).

This document validates the approach of using FRP for emission estimation on a global scale and characterises the GFASv0 data with the purposes of (1) providing users with an accuracy estimate for the current product and (2) guiding the future developments of the fire component in MACC.

Section 2 introduces the datasets used in this study. Section 3 assesses the availability of the FRP observation system for the calculation of fire emissions in real time. Section 4 compares estimates of dry matter burned from the most recent Global Fire Emission Database (Version GFED3.1; van der Werf et al., 2010) with corresponding data derived from FRP observations by the MODIS instruments. Section 5 compares GFASv0 emission estimates of carbon monoxide (CO) with those of the GFED inventory. Section 6 summarises a comparison of agricultural waste burning emission estimates from GFED on the one hand and based on national reporting on the other. Section 0 depicts an example from atmospheric composition forecasting based on GFASv0. Finally, Section 8 formulates recommendations for the further development of the MACC fire emission service. The annex provides a brief overview of the use history of fire products in MACC.

2 Datasets

2.1 GFED

The Global Fire Emissions Database (GFED) is a set of monthly fire emissions estimates that originated from studying the role of fire in the terrestrial carbon cycle. Over the years the modelling framework has been refined to serve the needs of the atmospheric science community and emissions estimates are in use by over 100 research groups around the world. The first version was released in 2004 (van der Werf et al., 2004) followed by GFED2 in 2006 (van der Werf et al., 2006). In the MACC starting phase, GFED2 was used in several ways, most importantly to scale GFASv0 to achieve global emissions similar to GFED2. In the meantime, the third version of GFED has been finalized. This version is already used in several parts in this report and will be used to further refine GFAS. A preliminary version (GFED3.0) has been used but will be replaced by GFED3.1. Main improvements of GFED3 with respect to GFED2 are summarized in Table 2-1 and in van der Werf et al. (2010). GFED is based on the Seiler and Crutzen (1980) approach to assess emissions; combining estimates of burned area, fuel loads (biomass), and the fraction of fuel that is actually combusted during the fire, the so-called combustion completeness. This is done for each 0.5° grid cell and month with most input datasets derived from satellite retrievals.

Parameter	Description of modification	Impact on model estimates
Burned area	We now primarily use 500 meter burned area maps from MODIS during 2001-2009 instead of regional relationships between fire hot spots and burned area	Estimates of burned area significantly improved in North America (Giglio et al., 2010); fire emissions estimates are no longer impacted by regional variations in fire hot spot to burned area relationships.
Spatial resolution	Increased from 1° to 0.5°	Factor of 4 increase in spatial resolution; smaller errors due to heterogeneity in landscape
Leaf senescence	Reduced carry-over of leaves during the dry season to the following wet season in herbaceous vegetation	Decreased biomass in herbaceous fuels, more in line with measurements
NPP allocation	Changed from a fixed to a dynamic allocation based on mean annual precipitation	Better representation of spatial variability in aboveground biomass in highly productive ecosystems
Sub-grid cell information on burned area distribution over land cover and fractional tree cover bins	Changed from uniform distribution of burned area to herbaceous and woody fuel classes to dynamic distribution based on sub-grid cell information	Improved representation of spatial and temporal variability in fuel type burning and mortality rates; better ability to apply emission factors
Deforestation rates	Previous calculation based solely on burned area changed to combine burned area in wooded ecosystems and fire hot spot persistence	Ability to separately estimate deforestation emissions; fuel loads in deforestation regions are no longer impacted by other fire activity in the grid cell (e.g., agricultural maintenance fires)
Deforestation emissions	Newly introduced; deforestation emissions based on clearing rates in the wooded fraction of the grid cell	New insights into deforestation fire activity; ability to track deforested land through time to calculate emissions from respiration (forthcoming work)
Uncertainty	Assessment of uncertainties	Monte Carlo approach provides insight into the spatial and temporal variability in global fire emissions.

Table 2-1: Improvements in biogeochemical modeling framework for GFED3 with respect to GFED2.

2.1.1 Burned area

GFED3 is based on the Giglio et al. (2010) burned area time series; which was built using four satellite data sets. At the core lies a 500 meter burned area mapping algorithm based on a burn-sensitive vegetation index, with dynamic thresholds aided by active fires, and applied to MODIS imagery (Giglio et al., 2009). Over 90% of the area burned used in GFED3 over 2001-2009 was mapped this way. Local and regional scale relationships between MODIS active fires and burned area were used to map remaining areas in the MODIS era, while a mix of VIRS (Giglio et al., 2003) and ATSR (Arino et al., 1999) active fire data were used to map pre-MODIS era burned area in a similar way. Several corrections were made to arrive at a consistent, long-term burned area dataset, see Giglio et al. (2010) for more details. This new burned area data set compares well to independent burned area estimates for North America, as well as to subsets of burned area derived from Landsat in tropical regions (Giglio et al., 2009).

2.1.2 *Fuel loads and combustion completeness in the CASA model*

CASA calculates carbon 'pools' for each grid cell and time step based on carbon input from net primary productivity (NPP) and carbon emissions through heterotrophic respiration (Rh), fires, herbivory, and fuelwood collection. NPP was calculated based on satellite-derived estimates of the fraction of available photosynthetically active radiation (fAPAR) absorbed by plants:

$$NPP = fAPAR \times PAR \times \varepsilon_{(T,P)} \quad (1)$$

where PAR is photosynthetically active radiation, and ε is the maximum light use efficiency (LUE) that is downscaled when temperature (T) or moisture (P) conditions are not optimal. NPP was delivered to living biomass pools (leaves and roots for herbaceous vegetation, and leaves, roots, and stems for woody vegetation) following the Hui and Jackson (2005) allocation scheme with more NPP delivered to leaves and stems when mean annual precipitation (MAP) is high while larger amounts of NPP are delivered to roots when MAP is low (ter Steege et al., 2006).

Carbon in the living biomass pools was transferred to litter pools depending on turnover rates and satellite-derived changes in fAPAR (Randerson et al. 1996) and subsequently decomposed based on turnover times regulated by temperature and moisture conditions (Potter et al., 1993). Other loss pathways include herbivory based on empirical relations between NPP and herbivore consumption (McNaughton et al., 1989) and fuelwood collection based on national fuelwood use statistics and population densities (following van der Werf et al., 2003).

Fuel type	CC_{min}	CC_{max}	Max. burn depth (cm)
Leaves	0.8	1.0	-
Stems	0.2	0.4	-
Fine leaf litter	0.9	1.0	-
Coarse woody debris	0.4	0.6	-
Boreal organic soil matter	-	-	15
Tropical peat organic soils	-	-	50

Table 2-2: Minimum and maximum combustion completeness (CC, unitless) or maximum burn depth for different fuel types (cm).

For each grid cell and month, fire carbon emissions were then based on burned area, tree mortality, and the fraction of each carbon pool combusted (combustion completeness, CC). Each carbon pool was assigned a unique minimum and maximum CC value with the fine fuels (leaves, fine litter) having relatively high values while coarse fuels (stems, coarse woody debris) having lower values (Table 2-2). The actual combustion completeness was then scaled linearly based on moisture conditions with CC closer to the minimum value under relatively moist conditions, and vice versa (see van der Werf et al., 2006 for more details).

2.1.3 *Brief overview of global results*

Below we will focus on carbon emissions, but spatial and temporal variability for trace gas and aerosol emission is highly related to carbon emissions. According to GFED3, average carbon emissions over 1997-2009 were 2.0 Pg C $year^{-1}$ with considerable interannual variability, especially over the 1997-2001 period (Table 2-3). Emissions in the peak fire year 1998 (2.8 Pg year-1) were 70% higher than

those in 2001 (1.6 Pg year^{-1}). From 2002 through 2007, emissions were relatively constant from year to year on a global scale. Regionally, however, large variations occurred but high fire years in some regions cancelled low fire years in other regions. In 2006 for example, emissions in southern hemisphere South America were relatively low while in equatorial Asia (EQAS) emissions were higher than in any other year except 1997. In 2007 the reverse occurred with high emissions in southern hemisphere South America and low emissions in EQAS. In 2008, almost all regions experienced below average emissions with the notable exception of boreal Asia, leading to a relatively low fire year globally (1.7 Pg year^{-1}). This situation persisted in 2009, although boreal Asia was now also low while emissions in equatorial Asia increased somewhat, leading to the year with lowest emission over 1997-2009 with 1.5 Pg year^{-1}.

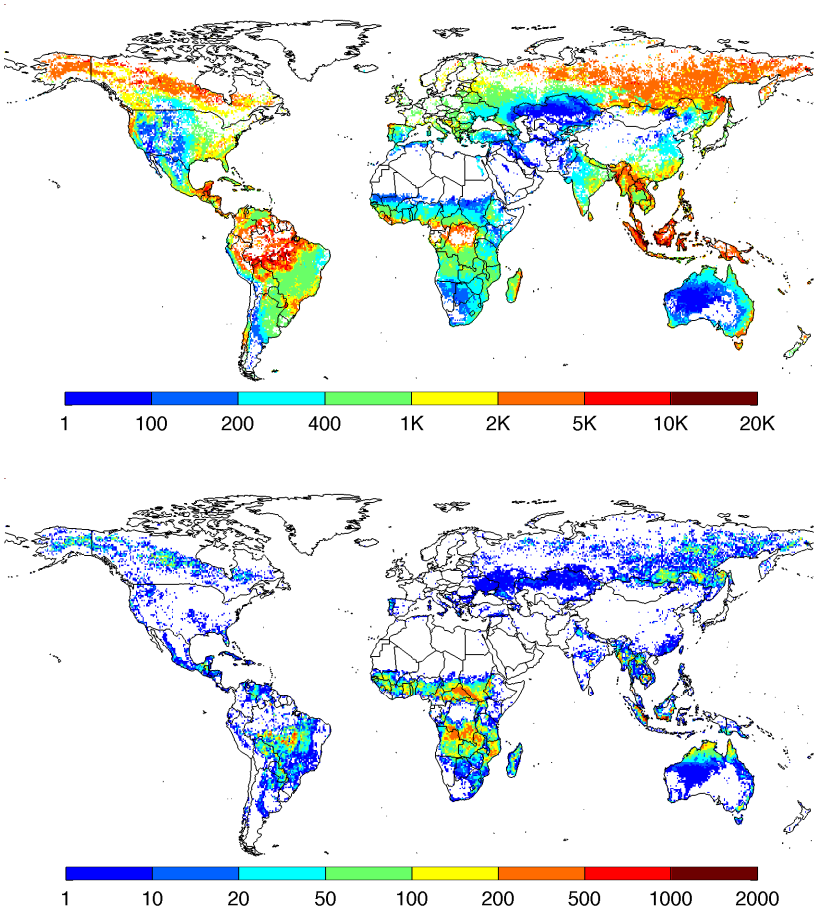

Figure 2-1: Fuel consumption (top, g C per m^2 of burned area) and mean annual fire carbon emissions (bottom, g C m^{-2} year^{-1}). Both plots show data averaged over 1997-2009. Fire carbon emissions are the product of the fuel consumption shown in the left-hand panel and the burned fraction of the grid cell.

Almost half of the global carbon emissions were from Africa, with emissions from Africa south of the equator (26%) slightly exceeding those from northern hemisphere Africa (23%). South America accounted for 17% of global carbon emissions, mostly from southern hemisphere South America. On average, Equatoria Asia is the fourth most important region (10%) with its relative contribution growing considerably during El Niño years. In 1997, for example, we estimated that emissions from this region contributed to 39% of global emissions. According to our estimates, the boreal region accounted for 9% of total global carbon emissions, with emissions from boreal Asia almost 2.5 times

as high as those from boreal North America and comparable to emissions from Australia. While the Scandinavian countries and Finland were not included in the boreal region in our assessment, emissions here were negligible when compared to boreal North America and Asia.

Results of Monte Carlo simulations indicate that globally, uncertainties were around 20% (1sigma) for annual estimates during the MODIS era (2001 – 2009).

Region	Year													Mean	Contribution (%)
	1997	1998	1999	2000	2001	2002	2003	2004	2005	2006	2007	2008	2009		
BONA	19	116	36	14	5	69	60	139	66	50	40	49	44	54	2.7
TENA	2	8	11	12	6	10	9	4	6	11	20	13	8	9	0.5
CEAM	14	60	14	27	9	13	28	8	27	20	14	14	19	20	1.0
NHSA	20	51	14	19	17	9	54	26	13	11	25	13	13	22	1.1
SHSA	201	412	298	137	143	231	214	327	459	241	572	194	91	271	13.4
EURO	4	6	3	9	5	2	5	3	5	4	7	2	2	4	0.2
MIDE	1	2	2	1	2	2	2	2	1	2	3	1	2	2	0.1
NHAF	581	586	511	532	428	479	506	407	532	442	441	445	362	481	23.9
SHAF	514	682	534	514	514	483	597	579	621	548	533	578	544	557	27.7
BOAS	42	338	85	141	103	191	333	16	48	96	46	165	66	128	6.4
TEAS	57	31	18	37	33	49	43	25	27	35	35	40	31	36	1.8
CEAS	65	187	160	56	40	91	69	166	87	83	165	64	106	103	5.1
EQAS	1069	184	33	21	70	285	71	109	123	368	21	25	101	191	9.5
AUST	118	112	182	146	186	153	128	155	89	147	122	78	136	135	6.7
Global	**2705**	**2775**	**1901**	**1665**	**1561**	**2066**	**2118**	**1966**	**2105**	**2059**	**2043**	**1681**	**1524**	**2013**	**100.0**

Table 2-3: Annual emissions estimates (Tg C year^{-1}) over 1997 – 2009 for different regions where BONA is Boreal North America, TENA is Temperate North America, CEAM is Central America, NHSA is Northern Hemisphere South America, SHSA is Southern Hemisphere South America, EURO is Europe, MIDE is Middle East, NHAF is Northern Hemisphere Africa, SHAF is Southern Hemisphere Africa, BOAS is Boreal Asia, CEAS is Central Asia, SEAS is Southeast Asia, EQAS is Equatorial Asia, and AUST is Australia and New Zealand.

Regional differences between GFED2 and GFED3 are generally within plus or minus 40% when expressed as carbon monoxide emissions (Figure 2-2). However, larger positive differences occur for boreal North America, Middle East and occasionally in Equatorial Asia, while negative differences of more than -40% occur in Temperate North America, Central America, Europe and occasionally in a few other regions.

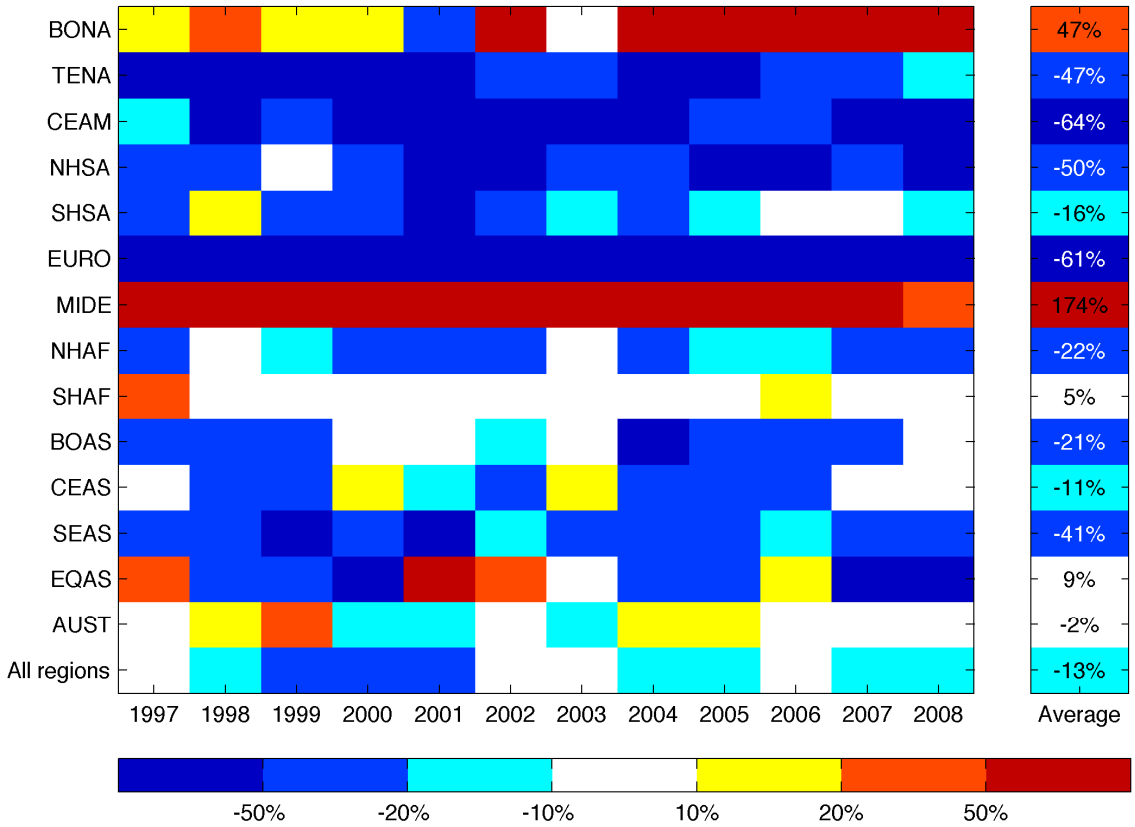

Figure 2-2: Differences in fire carbon monoxide (CO) emissions estimates between GFED3 and GFED2, as a percent of GFED2 estimates. Positive numbers indicate GFED3 is higher than GFED2 and vice versa. Region abbreviations explained in Table 2-3.

2.2 GFASv0

The current version of the MACC Global Fire Assimilation System, GFASv0, produces real time biomass burning emissions estimates based on satellite-derived FRP observations. The observations currently come from the geostationary Meteosat SEVIRI (located over Africa and which also views Europe and parts of south America, albeit at large view zenith angles) and the two polar-orbiting MODIS instruments (which provide global observations, though with a repetition frequency far lower than that of SEVIRI). The methodology is described in detail in Kaiser et al. (2009a) and Kaiser et al. (2009b). It comprises the following steps:

1. The FRP values and locations of observed fire pixels are extracted from the MOD14/MYD14 and FRPPIXEL_List products for the MODIS and SEVIRI satellite sensors, respectively.
2. The location of pixels with observed FRP=0 are extracted from the MOD14/MYD14 in conjunction with the MOD03/MYD03 products for MODIS FRP and from the FRPPIXEL_Quality product in conjunction with static geolocation data for SEVIRI.
3. For each instrument, the observed values of FRP ≥ 0 are averaged in each cell of a global T159 grid, which has about 125 km resolution. Thus the observed distribution of fires in the cloud-free land pixels is assumed to be representative for the FRP density ρ [W m^{-2}] of the whole grid cell. At the coastline, the average is also scaled with the land fraction of the grid cell to account for the prior knowledge that fires on water surfaces are not due to vegetation burning (there is a potential for off-shore oil flaring fires to be detected in the retrieval).

4. For SEVIRI, the FRP density field is increased twofold to adjust for omitted fires with FRP below the instrument's detection threshold.

5. For each instrument, the footprint areas of the pixels with observed values of FRP ≥ 0 are summed in each global grid cell. The sum a [m^2] is interpreted as quantitative measure for the accuracy of the observed FRP density field.

6. The steps above are performed for each individual satellite fire product. The resulting fields of FRP density ρ are averaged for a single day to obtain the daily FRP density. The averaging is performed with weights prescribed by the observed area sums a. The weighing fills in observational gaps in space and time and also yields observed area fields for the entire day, which can be compared to grid cell sizes to obtain the effective observation frequency or period.

7. The daily FRP density field is scaled with a global factor of $1.37 \cdot 10^{-6}$ kg DM J^{-1} to obtain the dry matter combustion rate and further with land cover specific emission factors to obtain the emissions of various species. The global scaling factor has been selected such that the global emissions calculated by GFAS for 1 Oct 2008 – 17 Jun 2009 equal the average of the corresponding emission fluxes in GFED2 during the years 2000-2007 (Kaiser et al. 2009a). The emission factors of GFED2 are used and land cover is divided into the three classes; "savanna", "tropical forest" and "other forest".

2.3 MODIS FRP

The MODIS fire products MOD14/MYD14 for the time period 2003-2008 were downloaded from the NASA data archive. MACC has also archived the MODIS fire products obtained since October 2008 in real time. Thus MACC has a complete time series of MODIS fire observations dating back to 2003. The MODIS products were reprocessed for the full time period 2003-2009 with a re-engineered processing chain of the GFAS to obtain a long time series of FRP fields. The re-engineering was primarily carried out to allow the GFAS to run with full operational support on ECMWF's high performance computing facility. It also incorporates several technical and scientific optimisations. The differences to the methodology described above are:

Step 1. No change.

Step 2. The locations of MODIS pixels with observed FRP = 0 are calculated from the granule corner coordinates extracted from MOD14/MYD14 using a custom interpolation routine. This is necessary because the MOD03/MYD03 product has such a large volume that it cannot be downloaded from NASA for time periods of several years. The interpolation has an accuracy of typically 5 – 10 km. Errors of up to 25 km have been found, though.

Step 3. A regular latitude-longitude grid with 0.1 deg resolution is used.

Step 4. N/A

Step 5. Each pixels footprint area is scaled with $\cos^2$ (view_zenith_angle) before summation. This represents to some degree the decrease of the FRP accuracy towards the MODIS swath edges. The sum is also scaled with the global grid cell area, so that it represents the observed fraction of the grid cell.

Step 6. No change.

Step 7. N/A

In order to compensate further for persistent observational gaps, one processing step has been added:

Step 8. The daily FRP density fields are smoothed with a running 5-day window. The smoothing is implemented as weighted averaging with weights given by:

a. The observed fraction of the grid cell for the middle day.

b. The observed fraction of the grid cell times 0.1 for its direct neighbours.

c. The observed fraction of the grid cell times 0.01 for the first and last day.

Thus the FRP density of a grid cell is only altered strongly when it is poorly observed on the day and well observed on any of the other days in the window.

3 Availability of FRP for Global Fire Emission Estimation

The FRPPIXEL product from SEVIRI is produced by the EUMETSAT LandSAF within 30 minutes of observations and distributed via EUMETCast. The MODIS fire products are produced by NASA within about 4 hours of observation and made available on a ftp server (ftp://nanuk.eosdis.nasa.gov). Therefore, both products are suitable for real time production of fire emissions estimates. The daily FRP and fire emission products are made available by MACC at 5 UTC for the preceding day.

The observational coverage achieved by MODIS and SEVIRI in GFASv0 is illustrated in Figure 3-1 with effective observation return periods calculated from daily observed area fields. It confirms that the polar-orbiting MODIS instruments achieve almost global coverage, but not completely. The observational gaps in areas with biomass burning are caused by persistent cloud cover. Areas with snow and ice cover are additionally excluded. The surprisingly small observation period values are partly due to multiple observations near the swath edges during a single overpass, i.e. the MODIS "butterfly" or "bow-tie" effect that results from along-track overlapping of edge-of-swath MODIS pixels. This is apparent in the stripy features.

The observation return periods of SEVIRI exhibit the same observational gaps due to cloud cover as does MODIS, albeit to a lesser degree due to its generally much shorter observation return period (15 mins from geostationary orbit). This also enables resolution of the diurnal cycle of biomass burning over most of the observed disk. Fire observations from further geostationary satellites will need to be added to GFAS in future to allow the overall time resolution to be lowered to one hour. FRP products from the GOES satellites, and possibly MTSAT, are therefore under development in MACC.

Figure 3-2 shows the daily coverage of the observations made by the two MODIS instruments in arbitrary units. The seasonal cycles of both data sets reflect the globally larger snow/ice-free land area in boreal summer. The coverage of the real-time products used for 2009 also exhibits somewhat larger scattering than that of the reprocessed products used during 2003-2008. This is to be expected given the operational constraints of real time production. The daily data set without smoothing exhibits a few individual days with strongly reduced or even vanishing coverage, which are caused by brief outages of the observing system or real time processing chain. They highlight the need for filling in of observational coverage. The data set with smoothing / gap filling has generally larger values by about 20%, which reflects the additional information derived from neighboring days. All but one day (7 Sep 2004) contain at least some information on the FRP density field.

(a)

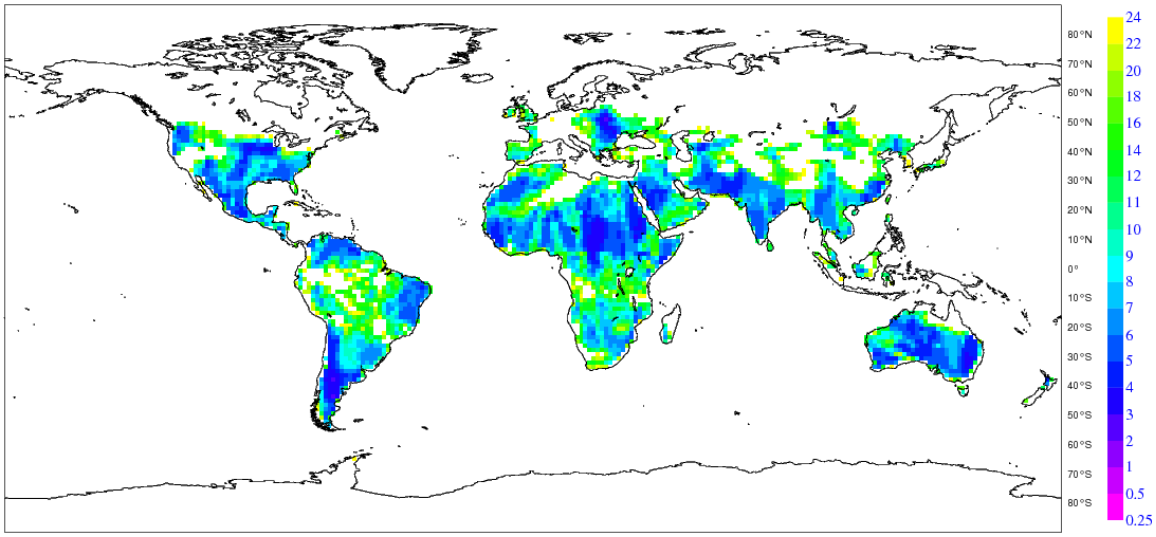

(b)

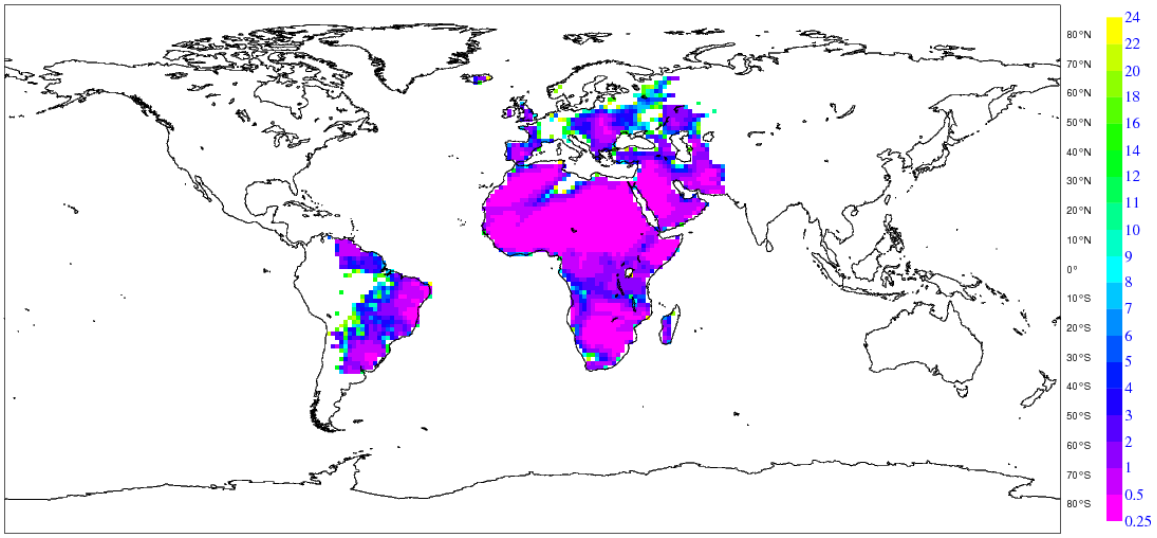

Figure 3-1: Indicative return periods (hours) for observations with the potential to detect a fire by (a) the two MODIS instruments and (b) SEVIRI on 7 February 2009.

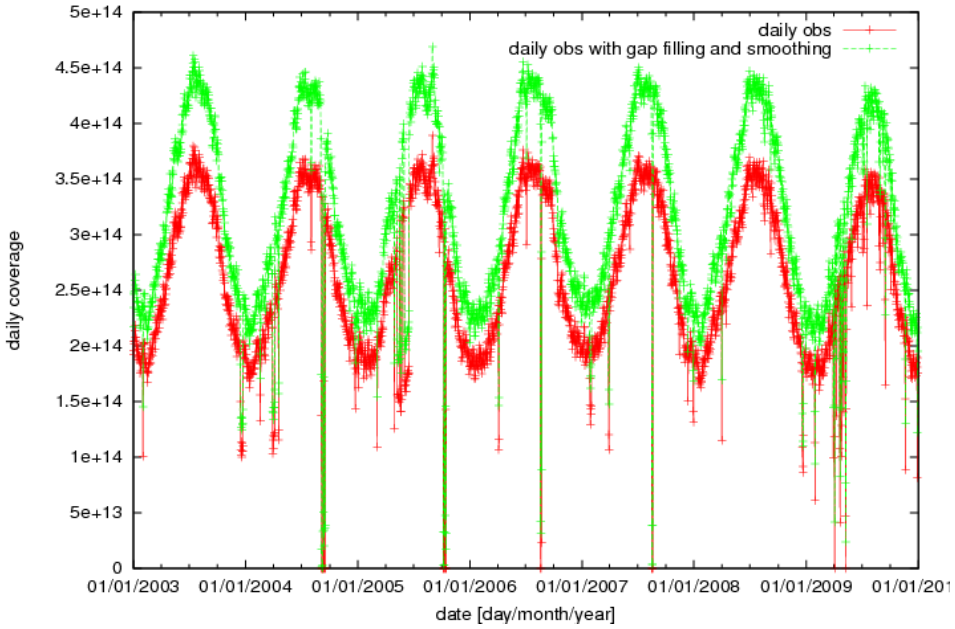

Figure 3-2: Daily coverage of the FRP ≥ 0 observations made by the two MODIS instruments in arbitrary units.

4 MODIS FRP vs. GFED3 Dry Matter Burned

4.1 Derivation of MODIS-FRP Dry Matter Burned

In the following section, we present the comparison of monthly mean MODIS FRP data with monthly GFED3.1 dry matter burned (DM) at a 0.5 degree horizontal resolution. To allow for a better comparability, MODIS-FRP data were converted into derived DM values using the empirical relationship between biomass combusted and fire radiative energy (FRE) as described in Wooster et al. (2005):

Biomass combusted (kg) = 0.368 FRE (MJ)

For simplicity, we assume that the biomass combusted calculated using this conversion factor (CF) of 0.368 [kg/MJ] corresponds to the amount of dry matter burned, thereby neglecting the water contained as fuel moisture. The fuel moisture of the Miscanthus grass used in the combustion experiment of Wooster et al (2005) ranged between 6 and 12%. However, fuel moisture exhibits strong spatiotemporal variations dependent on e.g. the relative humidity, preceding rainfall, temperature and fuel classes (e.g. fine or coarse fuels, living or dead biomass), which are not covered by the direct conversion of biomass combusted to dry matter burned. While fuel moisture of dead fine fuels is generally below 15% at environmental conditions typically prevailing during fires (relative humidity < 60%) (Pyne et al. 1996), it can, for example, exceed 200% in freshly flushed foliage (Nelson 2001).

With an average biomass moisture content of 20%, the CF published by Wooster et al. (2005) would correspond to a moisture adjusted CF (referring to DM burned) of 0.307 kg DM/MJ. A moisture adjusted CF close to 0.3 has also been found in more recent combustion experiments conducted by M. Wooster and colleagues. In contrast, Freeborn et al. (2007) yielded a moisture adjusted CF of 0.453 ± 0.068 kg DM/MJ from combustion experiments covering various fuel types. Given these uncertainties, we have chosen a moisture adjusted CF of 0.368 as an intermediate estimate.

For the assessment of fuel-type dependent differences in the estimated amount of dry matter burned, the distribution of predominant vegetation types was derived from the GFED3 fractional vegetation cover map (Figure 4-1). It comprises the major vegetation types: savanna (SA), agriculture (AG), tropical forest (TF), extratropical forest (EF), and tropical peat (PE). Here, peat is treated as predominant vegetation type, although - strictly speaking - it is a soil type. In GFED3, peat (PE) as predominant vegetation cover only occurs in Indonesia (southeastern Sumatra and southern Kalimantan).

GFED3 also maps areas where fires may consume part of the organic soil matter (OS) in addition to PE. These areas are restricted to the northern latitudes and are most prominent in the boreal zone. For the assessment of fuel-type dependent differences in this study, we separate these areas from those with no potential consumption of OS by fires. Potential consumption of OS by fires occurs in vast areas predominantly covered with extratropical forest (EFOS) (in total 67% of the area covered by EF). 10% of the areas with predominant savanna surface vegetation (SA) exhibit potential OS consumption (SAOS) and only 1% of the areas covered by AG (AGOS).

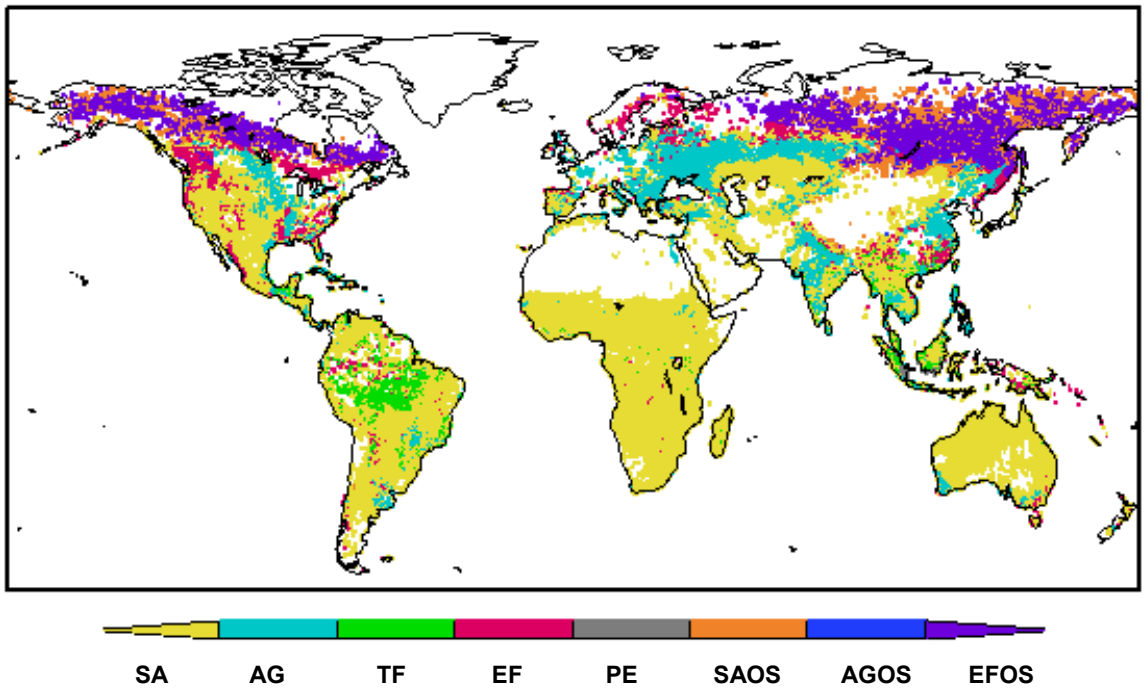

Figure 4-1: GFED3 predominant vegetation type map with savanna (SA), agriculture (AG), tropical forest (TF), extratropical forest (EF). Areas with potential consumption of organic soil matter (OS) by fires are shown as separate categories for SA (SAOS), AG (AGOS) and EF (EFOS) in addition to tropical peat (PE).

4.2 Spatial Patterns

4.2.1 Annual Biomass Burned

The spatial pattern of annual DM burned averaged over the period 2003 to 2009 is shown in Figure 4-2. The figure illustrates that GFED3 (left) and MODIS-FRP (right) exhibit largely similar spatial patterns in terms of the regions of major burning, e.g. in Africa's savanna belt north and south of the Equator, the Amazon Basin, northwestern Australia. However, GFED3 yields distinctively higher

amounts of biomass burned per unit area in these regions than does MODIS-FRP. Also, the spatial gradients are

more pronounced in GFED3. Fire events, however, are distributed over much larger areas in the MODIS-FRP data, most of which burn only very little dry matter (<1 g DM m^{-2} $year^{-1}$). Such small values are indicative of irregular fire activity (only one or two years out of the 7 year period) or they can be a result of only a small fraction of the grid cell area being burned at a higher fuel consumption. In nature, fuel consumption levels this low would not allow a fire to spread.

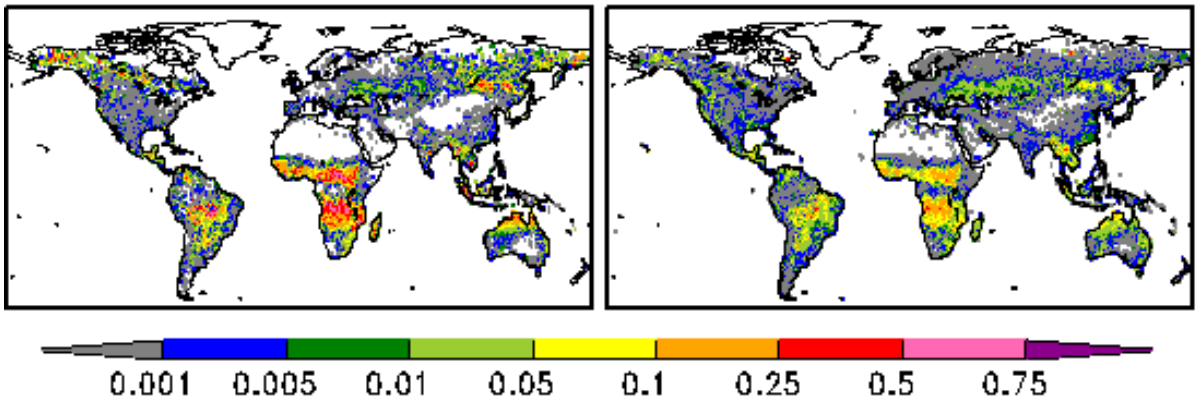

Figure 4-2 Mean total annual biomass burned (average over 2003-2009) (kg DM m-2 year-1) for GFED3 (left) and MODIS-FRP (right).

Figure 4-3 shows that the ratio GFED3 to MODIS-FRP dry matter burned exhibits distinct spatial features dependent on the predominant fuel type and the geographical position. Only in very few areas, the GFED3 to MODIS-FRP ratio is close to 1 (grey-colored grid cells with ratios between 0.7 and 1.4). In the vast majority, deviations are larger:

In the African savanna (SA) regions, the ratio is almost everywhere between 1.4 and 4. In the inner parts of South America covered by predominant savanna (SA) vegetation, the ratio scatters between 1.4 and 16. In northern Australia, the ratio is almost constantly between 1.4 and 2. In contrast, in predominant savanna (SA) or agricultural (AG) areas of North America and the Eurasian continent north of 30°N, the amount of biomass burned is generally distinctively lower in GFED3 than in MODIS-FRP. Over wide areas of North America, the ratio is below 0.125.

Australia shows a clear meridional trend from high (5-10) to low ratios (0.25). While the Australian continent is classified into savanna (SA) as predominant fuel type, the area contribution of woody (shrubs) or forested vegetation increases towards the north (see Figure 4-4, left). The meridional trend indicates that the GFED3 to MODIS-FRP DM ratio is high (above 1) in savanna regions with a substantial fraction of woody fuels (forests, woodlands) and low (below 1) in savanna regions with negligible contributions of woody fuels and lower biomass loads.

In regions covered by tropical forest (TF), GFED3 generally yields more than 2 times higher amounts of biomass burned than MODIS-FRP. In contrast, in regions covered by extratropical forest (EF), the GFED3 to MODIS-FRP ratio is mostly below 0.5, although there are also some scattered regions with ratios above 1.4.

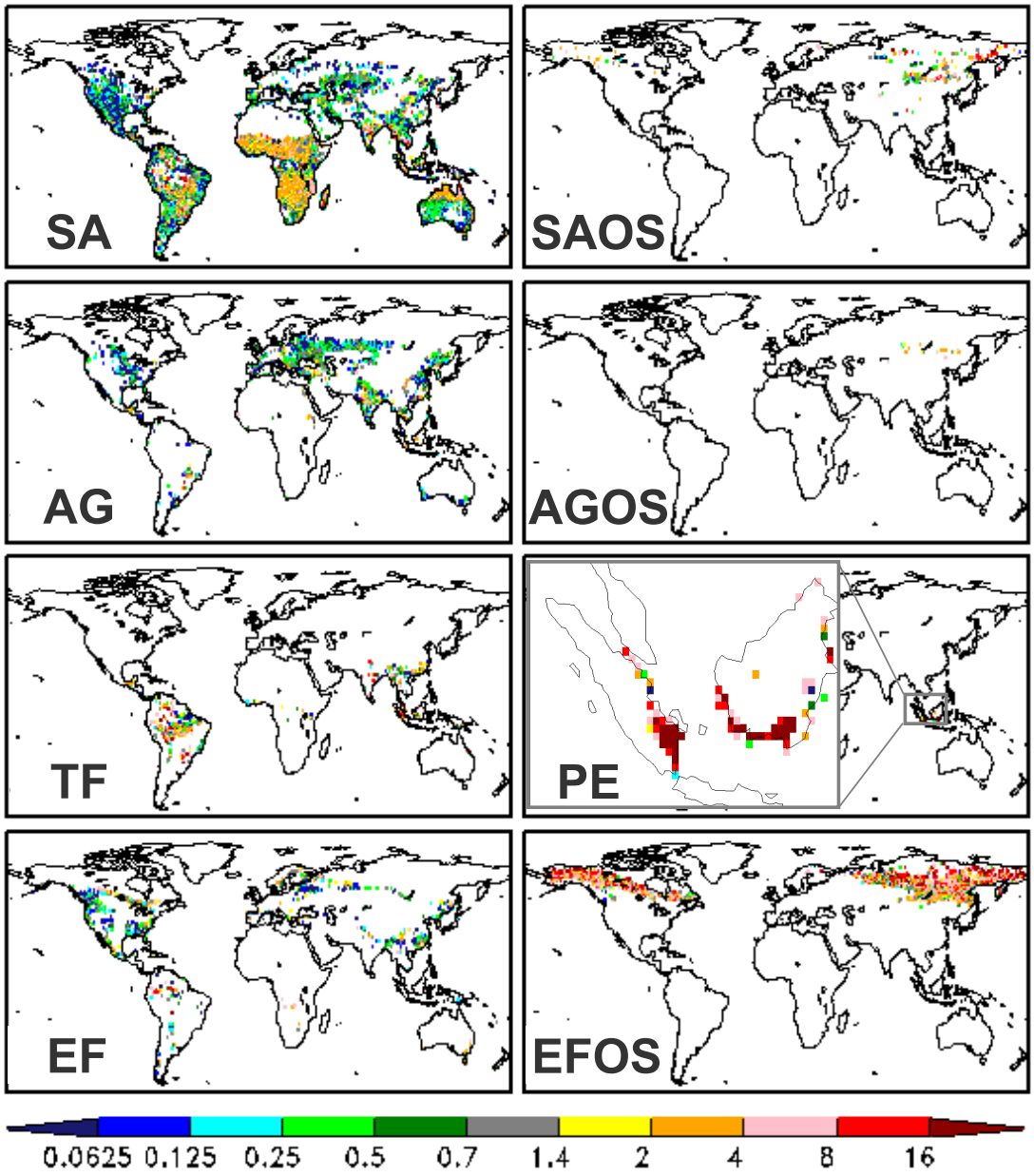

Figure 4-3: Ratio GFED3 to MODIS-FRP annual DM burned (average over 2003-2009), stratified by predominant surface fuel types (left column, SA=Savanna, AG=Agriculture, TF=Tropical Forest, EF=Extratropical Forest) and predominant surface fuel type with potential consumption of organic soil matter (OS)(right column, SAOS, AGOS, EFOS plus PE=Peat) (see Figure 4-1).

In regions with potential organic soil matter burning, i.e. regions characterized by a thick humus or peat layer (organic soil matter (OS) and peat (PE)), GFED3 yields distinctively higher amounts of dry matter burned than MODIS-FRP: in the boreal OS belt covered by extratropical forest (EFOS), the ratio is almost constantly above 4. In regions with tropical peat (PE) burning, the ratio is mostly greater than 16. Also in savanna and agricultural regions with potential organic soil matter burning (SAOS and AGOS), GFED3 also tends to yield higher DM values than MODIS-FRP, although the pattern is more heterogeneous.

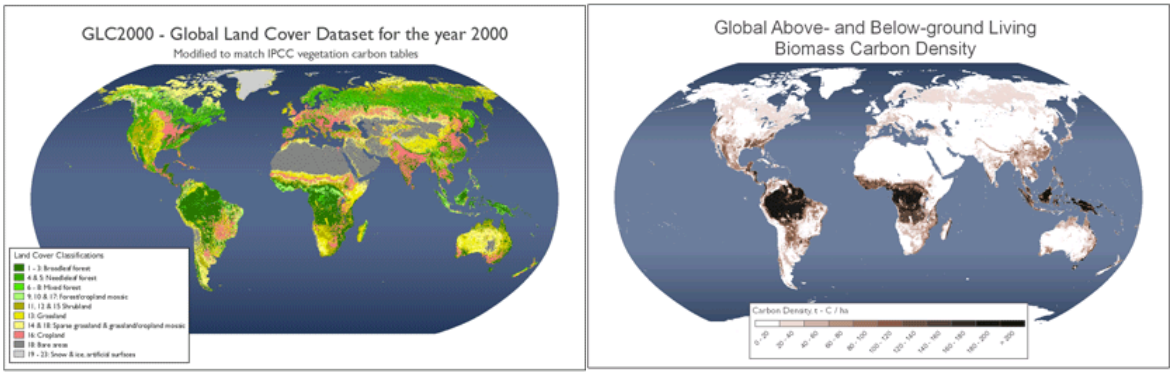

Figure 4-4: Global Land Cover (GLC 2000) map (left) and global map of estimated vegetation carbon stocks (right) available from http://cdiac.ornl.gov/epubs/ndp/global_carbon/carbon_documentation.htm l (Ruesch and Gibbs 2008).

In summary, GFED3 often yields distinctively higher amounts of dry matter burned per unit area than MODIS-FRP combined with the universal conversion factor of Wooster et al. (2005). The discrepancy is largest in regions where substantial burning of soil organic matter (organic soil matter (OS) or peat (PE)) occurs, which is characterized by slow, lower temperature combustion. Conversely, in regions with predominant savanna and agricultural areas outside the African savanna belt, MODIS-FRP yields higher dry matter burned per unit area than GFED3. In these regions, small fires with predominantly flaming combustion are common. The spatial pattern observed within a predominant fuel class (e.g. meridional trend of the GFED3 to MODIS-FRP ratio in northern Australia along with increasing contribution of woody fuels) indicates that the GFED3 to MODIS-FRP ratio may furthermore depend upon the fractional contribution of vegetation types within a grid cell. This dependency needs to be quantified in more detail in the next phase of the MACC project.

Finally, the comparison of GFED3 with MODIS-FRP indicates that dry matter burned may not be strictly proportional to observed FRP on the global scale. GFED3 to MODIS-FRP dry matter burned ratios distinctively above 1 may point to an underestimation of FRE e.g. due to an incomplete characterization of the temporal cycle of FRP (Ellicott et al. 2009) or the attenuation of the FRP signal by the atmosphere or the vegetation cover (Freeborn et al. 2008). It may also point to an overestimation of fuel loads in the GFED3 approach. Conversely, ratios distinctively below 1 may hint to an underestimation of dry matter burned by GFED3, e.g. due to low biased fuel loads, combustion completeness or burned areas. Fuel-class dependent differences of GFED3 and MODIS-FRP dry matter burned are discussed in more detailed in the following sections.

4.2.2 Number of Fire Observations per Grid Cell and Spatial Matching of Fire Events

The analysis of number of months when fires are detected within a grid cell, N_{FIRE}, provides insights into whether fire events detected by GFED3 and MODIS-FRP in a given location are singular events, recurrent events or almost stationary. For most fire-prone regions it is generally assumed that a distinct seasonal cycle occurs so that fires should be observed only in about half of all observation months. Figure 4-5 shows the total number of months with fire observations over the period 2003 to 2009 (in total 84 months) and Figure 4-6 the MODIS-FRP to GFED3 ratio.

There are pronounced differences in N_{FIRE} detected by GFED3 and MODIS-FRP. Except for very few areas in the northern boreal zone, N_{FIRE} MODIS-FRP is higher than in GFED3. In large areas of North America, for example, N_{FIRE} MODIS-FRP is more than 4 times larger.

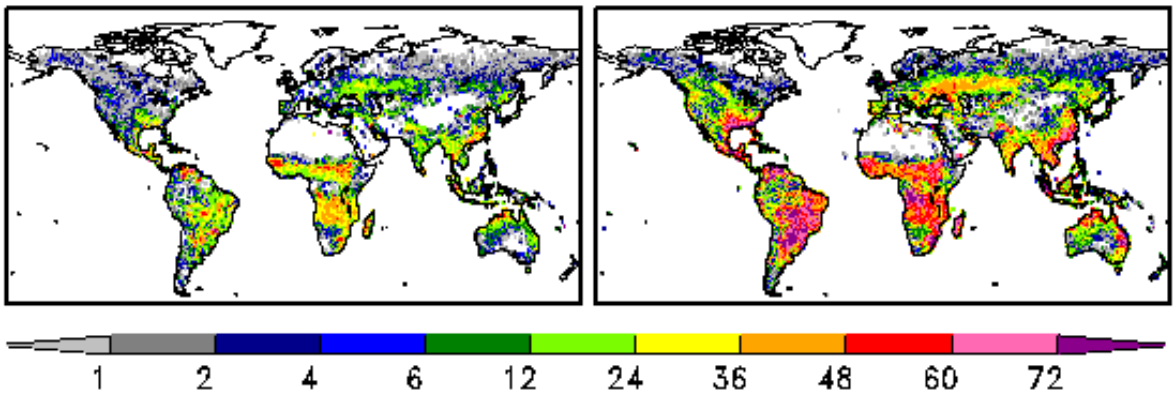

Figure 4-5: Total number of months with fire observations (NFIRE) over the period 2003 to 2009 (in total 84 months) detected by GFED3 (left) and MODIS-FRP (right).

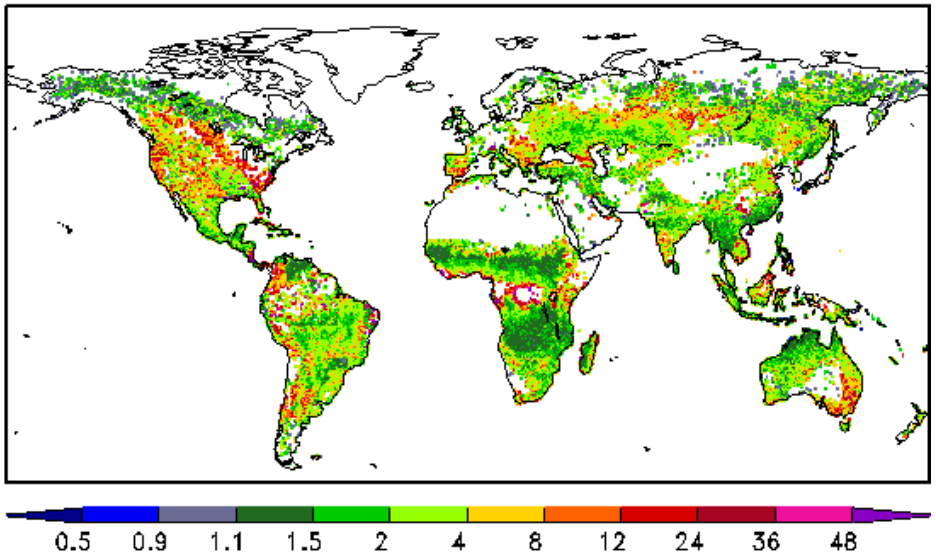

Figure 4-6: MODIS-FRP to GFED3 ratio of the total number of months with fire observations over the period 2003 to 2009 (in total 84 months) (see Figure 4-5).

In most of Brazil, but especially in Paraguay and northern Argentina, MODIS-FRP detects fires in more than 60 months out of the 84 months of the study period. Also GFED3 contains frequent fires here; however, the MODIS-FRP to GFED3 N_{FIRE} ratio is generally above 2. Most pronounced are the differences in central Equatorial Africa, where fires are almost stationary in MODIS-FRP (more than 72 months out of 84 months), while there are no or only very infrequent fires detected by GFED3.

There are a number of possible reasons for these discrepancies in the number of fire observations in each grid cell (N_{FIRE}):

Gas flaring:

The extraction of crude oil and natural gas often necessitates the burning of excess gas. This gas flaring happens quasi continuously and can be detected in satellite hot spot retrievals (Schultz, 2002).

These "stationary" fires are not removed from the original MODIS FRP product. While gas flaring detected by MODIS-FRP is an explanation for some of the detected quasi-stationary fires, they also occur in regions with no reported and/or very unlikely gas flaring (NOAA Gas Flaring report, Elvidge et al. 2009). A detailed analysis of the spatiotemporal patterns of possible gas flaring fires should be carried out in the next phase of the MACC project in order to mask out these fires.

Burned area versus hot spot detection:

The detection of burn scars from satellite images requires a much larger fraction (perhaps ~ 40%) of a pixel to be affected by fire than does the detection of fire hot spots (perhaps down to ~ 0.01 - 0.1%; Wooster et al. (2005)). The higher detection limit of the burn-scar based GFED3 (see also Section 5.1) may therefore partly explain why GFED3 has lower N_{FIRE}: some small fires in the MODIS-FRP dataset simply cannot be detected by GFED3. On the other hand it must also be noted that the burn scar retrieval is an integral measure (burned area over the entire fire duration), whereas detection of a hot spot necessitates the fire to be burning at the time of the satellite observation.

In order to shed some light on this issue we further analyzed the GFED3 non-detection areas (or GFED3 omission areas). Figure 4-7 illustrates that there are large areas, mainly on the American and the Eurasian continent, where fires are observed only in the MODIS-FRP product (seeFigure 4-1). In total, GFED3 does not detect fires in 33% of the 44931 grid cells with fire observation by MODIS-FRP. However, in most of these areas, the total number of the MODIS-FRP fires is low (less than 4 fire months from 2003 to 2009). These fires are generally small, with on average only 1 g m-2 year^{-1} of biomass burned, which is one order of magnitude lower than the global average of all MODIS-FRP fires. Provided that these MODIS FRP detections are real fires, this is an indication that the fires missed by GFED3 are small fires (e.g. agricultural burns) which contribute only rather little to the total biomass burned (< 4%) and will therefore have little impact on the overall fire emissions estimation. On the other hand, such fires may burn relatively close to population centres and could have a negative impact on air quality.

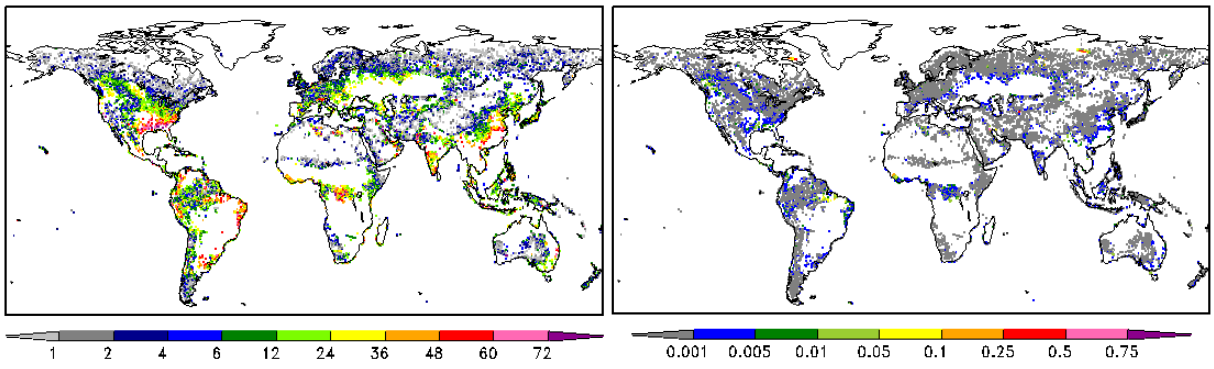

Figure 4-7: MODIS-FRP total number of months with fire observations (left) and mean annual total dry matter burned (right) over the period 2003 to 2009 for areas where no fires are detected by GFED3 (GFED3 non-detection areas).

Conversely, there is only a negligible area globally where GFED3 detects fires, but MODIS-FRP does not (22 grid cells out of 29680 cells with fire observations by GFED3, almost all off them in northern latitudes). This highlights the remarkable sensitivity of the MODIS sensor in detecting the presence of active fires.

False fire detections:

As the MODIS-FRP product used in this analysis contained all fire detections including those marked "low confidence", there were concerns that many of the small fires contained in the MODIS-FRP product but not in GFED3 are actually false fire detections. This concern was fuelled by the unexpectedly large number of monthly fire observations in each grid cell (N_{FIRE}) discussed above. Figure 4-8 compares monthly FRP budgets of several regions calculated from high-confidence fires with those calculated from all detected fires, i.e. high, nominal and low confidence. Generally, the contribution of fire detections with nominal and low confidence to the total FRP budget varies with time and region. However, in most regions these less certain fires mostly contribute about 1/3 to 1/4 throughout the year. North America constitutes notable exception to this general behaviour; during the fire season in late summer the vast majority of FRP is detected with high confidence, but during the winter low and nominal confidence fire detections are equally important. Thus at least some of the increased persistence (or reduced amplitude) of MODIS FRP in this region coincides with a reduction in MODIS fire detection confidence. The European fire season in April also displays a reduction in fire detection confidence. This is consistent with its interpretation as Eastern European agricultural waste burning with many small fires and lends some credibility to the MODIS FRP data including detections of any confidence. Further investigations are needed to confirm whether the detections with low confidence in particular yield information beyond that in GFED3. If they do not, then they should be excluded from the GFAS processing.

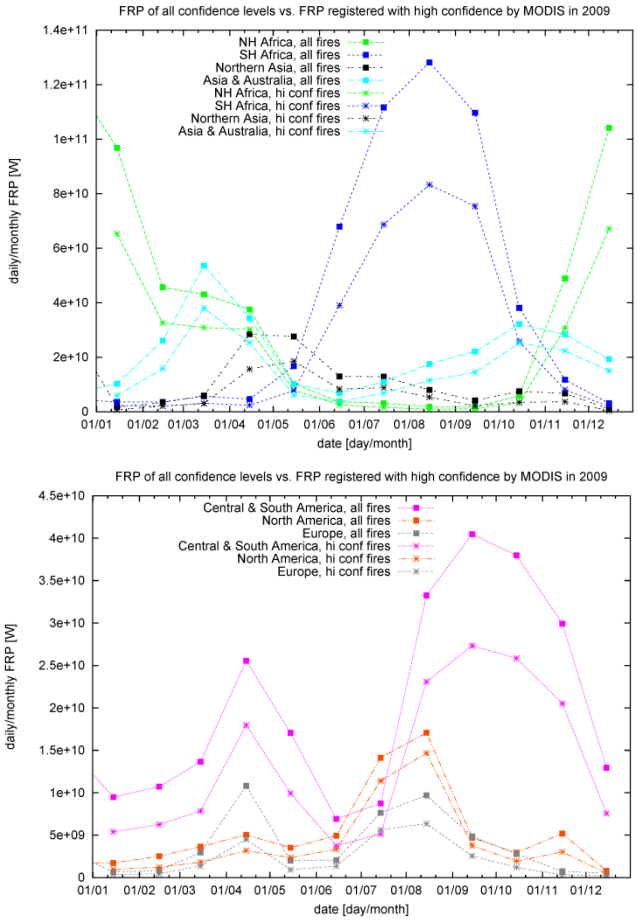

Figure 4-8: Monthly regional FRP budgets of 2009 calculated from all MODIS fire detections and calculated from MODIS fire detections with high confidence only.

4.3 Global and Regional Annual Totals

4.3.1 Annual Totals by Vegetation Type

Globally, GFED3 yields 2.2 times higher biomass burned than the direct translation of MODIS-FRP into biomass burned using the conversion factor (CF) defined in Wooster et al. (2005). Throughout the period 2003 to 2009, around 4 Gt DM was consumed by fires according to GFED3 compared to 1.8 Gt DM based on MODIS-FRP (Table 2-3). This mismatch was also found by other authors, e.g., Roberts and Wooster (2008) and Ellicott et al. (2009).

The ratio of dry matter burned calculated by GFED3 and MODIS-FRP is not constant, however. It is close to 1 in agricultural areas (AG) and extratropical forest (EF) with no potential consumption of organic soil (OS) matter. AG and EF fires, however, contribute less than 5% to the total amount of biomass burned. Around 74% of the burned biomass is burned in savanna (SA) areas (72% in the GFED3 and 76% in the MODIS-FRP estimate, respectively). Here, the GFED3 to MODIS-FRP ratio is on average 2.1. In tropical forests (TF), the mass ratio is close to 3.4. This vegetation types contributes between 8 and 12% (MODIS-FRP and GFED3, respectively) to the total biomass burned, respectively. Peat (PE) fires contribute 2.8% to the total biomass burned in GFED3 but are practically absent in the MODIS-FRP dataset (0.3% of the value estimated in GFED3 (global total). The GFED3 to MODIS-FRP ratio is on average 20 in the peat areas. In vegetated areas with potential burning of organic soil matter (OS) (i.e. SAOS, AGOS, EFOS), the ratios are generally distinctively higher than in the corresponding fuel class with no potential OS burning. The ratio for EFOS is 4.4 compared to 1.3 in EF. Fires in EFOS correspond to 4 to 8% (MODIS-FRP and GFED3, respectively) of the total dry matter burned while the contribution of SAOS and AGOS fire is less than 0.6%.

Thus, there is an apparent increase of the GFED3 to MODIS-FRP mass ratio in biomes with potential organic soil matter burning (OS and PE). Most striking is the difference between the ratio for tropical PE and the corresponding surface fuel type TF (ratio of 19.5 compared to 3.4). With the exception of EF, there is also an apparent increase in the ratio with increasing fuel loads of the predominant surface fuel type (i.e. from AG, GS to TF).

It is unlikely that the biomass burned estimates by GFED3 are biased high in the same order of magnitude as the GFED3 to MODIS-FRP mass ratio differs with different fuel types. High ratios are rather an indication for inherent limitations of the MODIS-FRP product used in this study to correctly quantify the FRP released by fires in particular ecosystems, i.e. notably in those with substantial subsurface fuels (OS or PE) and/or higher fuel loads.

A possible explanation for part of the underestimation of biomass burned in forested ecosystems relative to GFED3 is the obstruction or attenuation of the thermal signal produced by understory fires by the canopy cover (Freeborn et al. 2008). Since FRP relies on a measurement of the thermal radiation release by actively burning fuel, if this fuel is located under a dense tree canopy then the measurement is by definition likely to be low-biased. High-intensity, fast spreading crown fires account for the majority of the area burned in the boreal zone, particularly in North America (Kasischke et al. 2005). Kasischke et al. (2005) estimated that during the middle of the fire season, crown fires accounted for 40% of the area burned in boreal Russia and for 80% in boreal North America. Wooster and Zhang (2004) indicate that the MODIS FRP record also records substantial differences between these two areas. But even during a boreal crown fire, the crown fuel contributes only around 35% to the total amount of biomass combusted per unit area (Stocks and Kauffmann

1997). The largest fraction of the biomass consumed during a boreal crown fire (45%) emanates from burning of soil organic matter (ground fires), and the remainder (20%) from burning the litter layer and the undergrowth (surface fires) (Stocks and Kauffmann 1997). In contrast to extratropical forests, the majority of fires in undisturbed tropical forests predominantly burn in the litter layer and are neither fast-spreading nor intense (Cochrane 1999). Fire intensity in tropical forests, however, increases with preceding disturbances (number of preburns) (Cochrane 1999). The generally low GFED3 to MODIS-FRP dry matter burned ratios observed in North American regions with EF compared to the forested regions in the tropics (TF and EF) (Figure 4-3) could partly be explained by these differences in fire types.

Ground fires predominantly burn by smouldering combustion, with low fire line intensities (<10 KW m^{-1}) and peak temperatures generally around 500 °C (Ryan 2002). They typically keep burning for hours to weeks, frequently burning into the depth or progressing laterally below the topsoil layer (Usup et al. 2004). Temperatures at the soil's surface may not reach 200°C under such conditions. (Ryan 2002). In addition, the thermal signal of the ground fire could be obscured by overlaying ash, debris or surface vegetation. As a result, the thermal signal of these fires may be strongly attenuated, providing a possible explanation for the underestimation of biomass burned in biomes with substantial subsurface fuels (OS and PE) by MODIS-FRP relative to GFED3. This feature appears to be most pronounced in fires occurring in the tropical peatlands (PE) of Insular Southeast Asia (Figure 4-3). These organic soils allow for particularly sustained subsurface fires, burning up to metres into the depth (Ballhorn et al. 2009).

This analysis shows that the "smoldering effects of fires in FRP estimation" (Pereira et al. 2009) needs to be better studied and quantified. This will require extensive field work together with detailed analysis of the satellite data from such fires (cf. Kaiser et al. 2010).

Global statistics (period 2003-2009)		Fuel Class								
		SA	AG	TF	EF	SAOS	AGOS	PE	EFOS	ALL
DM burned (Gt year-1)	GFED3	2.9	0.1	0.5	0.1	0.0	0.0	0.1	0.3	4.0
	MODIS-FRP	1.4	0.1	0.1	0.1	0.0	0.0	0.0	0.1	1.8
	Ratio GEF3/ MODIS-FRP	2.1	0.9	3.4	1.3	2.4	3.6	19.5	4.4	2.2
% of all fuel types	GFED3	72%	2%	12%	2%	1%	0%	3%	8%	100%
	MODIS-FRP	76%	5%	8%	3%	1%	0%	0%	4%	100%
Linear regression monthly GFED3 DM with MODIS-FRP FRE	R^2	81%	54%	78%	44%	47%	76%	82%	88%	79%
	Slope (kg DM MJ-1)	1.06	0.22	1.34	0.63	0.88	1.56	9.38	1.70	1.19
	Intercept (kg DM month-1)	-90.7	2.8	-3.3	-1.8	0.0	-0.2	-2.9	-1.1	-155.0

Table 4-1: Summary statistics of global annual total biomass burned (mean over 2003-2009) estimated by the GFED3 and MODIS-FRP approach for different vegetation types (SA=Savanna, AG=Agriculture, TF=Tropical Forest, EF=Extratropical Forest) and predominant surface fuel type with potential consumption of organic soil matter (OS)(right column, SAOS, AGOS, EFOS plus PE=Peat).

Another factor that could be worth investigating is whether an adjustment of the atmospheric water vapor correction for the "fire moisture" improves the MODIS-FRP retrieval. Parmar et al. (2008) showed that fuel moisture can significantly contribute to the water vapor content of fire plumes and possibly to the formation of pyroclouds. In forested areas, and notably those with substantial burning of soil organic matter (duff, peat), fuels may contain a considerable amount of moisture during a fire event and thus may lead to a more pronounced increase in the atmospheric column water vapour content compared to savanna or agricultural fires. In addition, smouldering fires which typically occur in moist organic soil matter or litter release much higher amounts of fire aerosols than flaming fires. Both, increased water vapour content and smoke aerosols may lead to an attenuation of the thermal signal (Giglio et al. 2008).

While high GFED3 to MODIS-FRP dry matter ratios can be an indication for an obstruction or attenuation of the FRP signal, they may partly also hint to an overestimation by GFED3. Similarly, low ratios, as for example observed in North America covered by EF, may hint to a potential underestimation of dry matter burned by GFED3.

4.4 Temporal Patterns

4.4.1 Monthly Global Biomass Burned

On a global scale, monthly total biomass burned using the GFED3 and the MODIS-FRP approach show a largely consistent temporal pattern, although the values in GFED3 exhibit a much greater amplitude (Figure 4-9). While the seasonal minima of monthly global total biomass burned are relatively similar in both products (around 100 Tg DM month^{-1}), the maxima differ distinctively. While GFED3 maxima reach up to 900 Tg DM month $^{-1}$, they do not exceed 300 Tg DM month^{-1} with MODIS-FRP. Nevertheless, on a global scale 79% of the monthly variation in the global amount of GFED3 biomass burned can be explained by monthly variations in MODIS FRP (Figure 4-10).

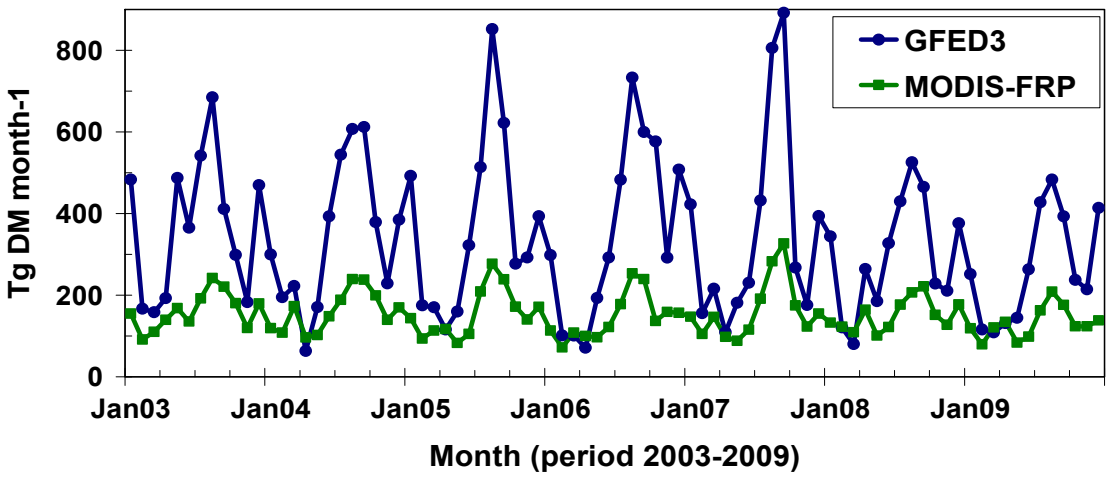

Figure 4-9: Time series of monthly global total biomass burned during 2003 to 2009 (Tg DM month^{-1}) estimated by the GFED3 and MODIS-FRP.

Linear regression (best-fit) of the monthly global total time series not only reveals this high coefficient of determination (R^2), but also provides an effective conversion factor (CF) of 1.2 kg DM/MJ FRE, which is around 3.3 times higher than the CF determined by Wooster et al. (2005) from small-scale experiments. Furthermore, the intercept of -155 Tg DM month^{-1} of the best-fit regression line can be interpreted as the cumulative effect of the lower-bound detection threshold of the GFED3 approach discussed in section 4.2.2.

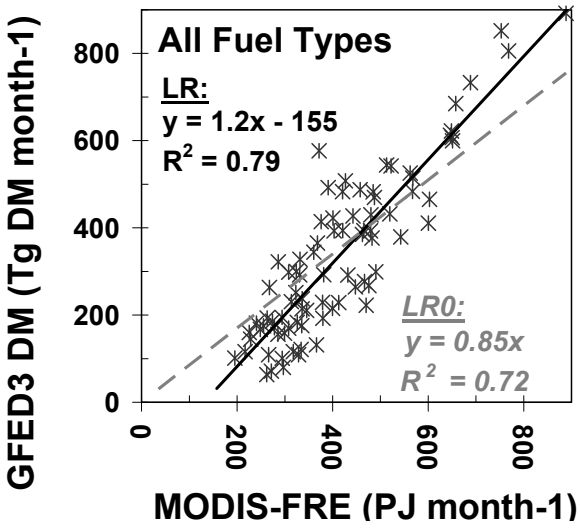

Figure 4-10: Linear regression (LR) of GFED3 monthly global total biomass burned during 2003 to 2009 (Tg DM month-1) with MODIS-FRP monthly global total fire radiative energy (FRE) (PJ FRE month-1). The figure shows a) the line of best fit (continuous black line) and b) the origin-forced line (dashed grey line). For both, the corresponding regression equation (y=mx+b) and coefficient of determination (R2) is given. The slope m of the equation corresponds to the conversion factor (CF) described in Wooster et al. (2005), see section 4.1.

The stratification of the linear regression by predominant fuel types shows a very high correlation for EFOS, PE, SA, TF and AGOS with coefficients of determination (R^2) between 0.76 and 0.88. For AG, SAOS and EF, the coefficient is lower (between 0.44 and 0.54). The slope of the linear regression line is by far highest in PE; the calculated effective conversion factor (CF) of 9.4 kg DM MJ^{-1} FRE is around 24 times larger than the CF described in Wooster et al. (2005). The effective CF is between 1.1 and 1.7 kg DM MJ^{-1} FRE in SA, TF, AGOS and EFOS, which is between 2.9 and 4.6 times higher than the CF described in Wooster et al. (2005).

The only effective CF smaller than the CF described in Wooster et al. (2005) is calculated for AG (0.22 DM MJ^{-1} FRE). For AG, also the only positive intercept is calculated (2.8 kg DM month^{-1}). These features could indicate an underestimation of dry matter burned in AG by GFED3, except for small AG fires . The linear regression also reveals a high negative intercept in predominant SA vegetation, pointing a lower-bound detection threshold of the GFED3 approach for savanna vegetation as discussed earlier.

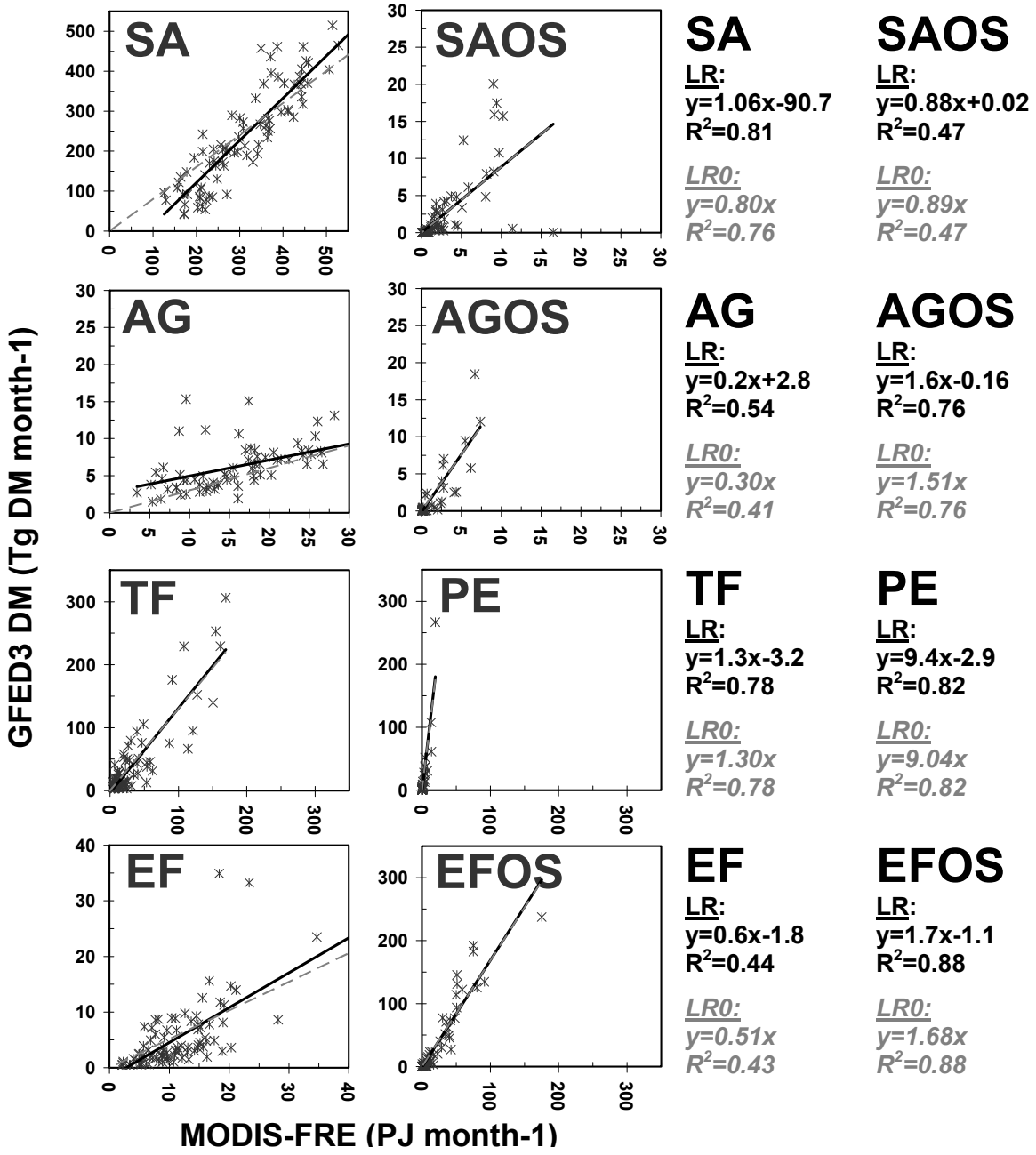

Figure 4-11: Same as Figure 4-10, but stratified by different fuel types.

4.4.2 Monthly Biomass Burned per Gridcell

Linear regression of monthly time series of GFED3 biomass burned with MODIS-FRP fire radiative energy (FRE) was also performed for each grid cell. The spatial plot of the coefficient of determinations shows that temporal similarities of both series are strongly dependent on the region and the fuel type.

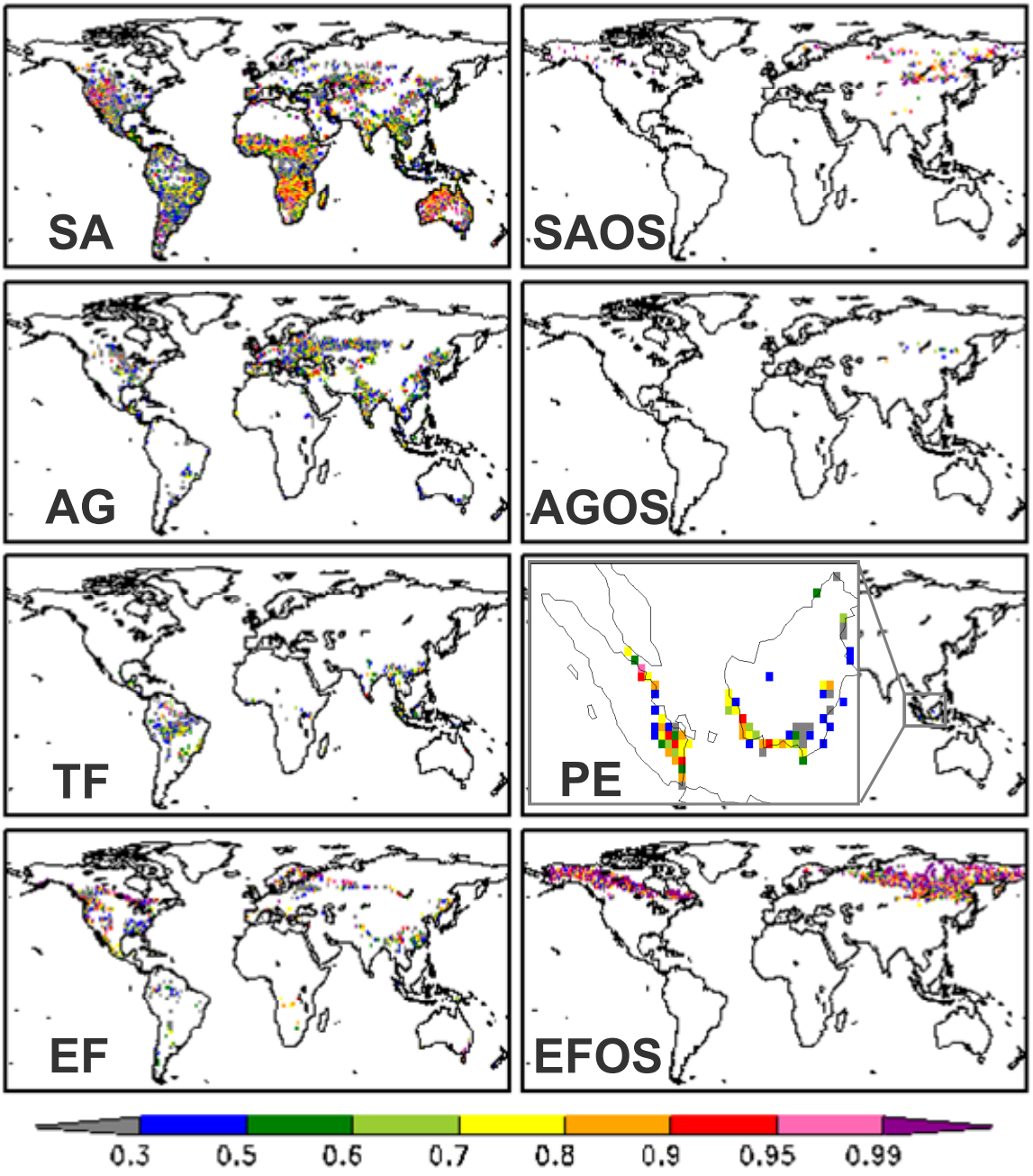

Figure 4-12: Coefficient of determination (R^2) calculated from the linear correlation of monthly GFED3 dry matter burned with MODIS-FRP observations over the period 2003 to 2009 (n=84), stratified by fuel types.

Almost throughout the entire boreal belt covered by EFOS, but notably in North America, GFED3 and MODIS-FRP monthly dry matter burned is very highly correlated. On average, however, GFED3 dry matter burned is 4.4 times higher than MODIS-FRP in this area (Table 4-1). Apparently, the relative difference between both datasets is very constant over time. Very high correlation coefficients are also found in almost the entire Australia, for large areas in western North America and the savanna regions of Africa, while they are generally lower and more spatially heterogeneous in South America and the Eurasian continent, except for areas covered by EFOS: Despite the high temporal correlation of the area totals in PE (R^2=0.88) (Table 4-1), the spatial pattern of the coefficient of determination is very

heterogenous with relatively low values (R^2<0.3) occurring in the large peat deposits of southern Kalimantan. Also in regions covered by predominant TF, the spatial correlation coefficients are generally relatively low (R^2<0.6) and spatially heterogeneous. Yet, the coefficient of determination (R^2) of the area totals is 0.78.

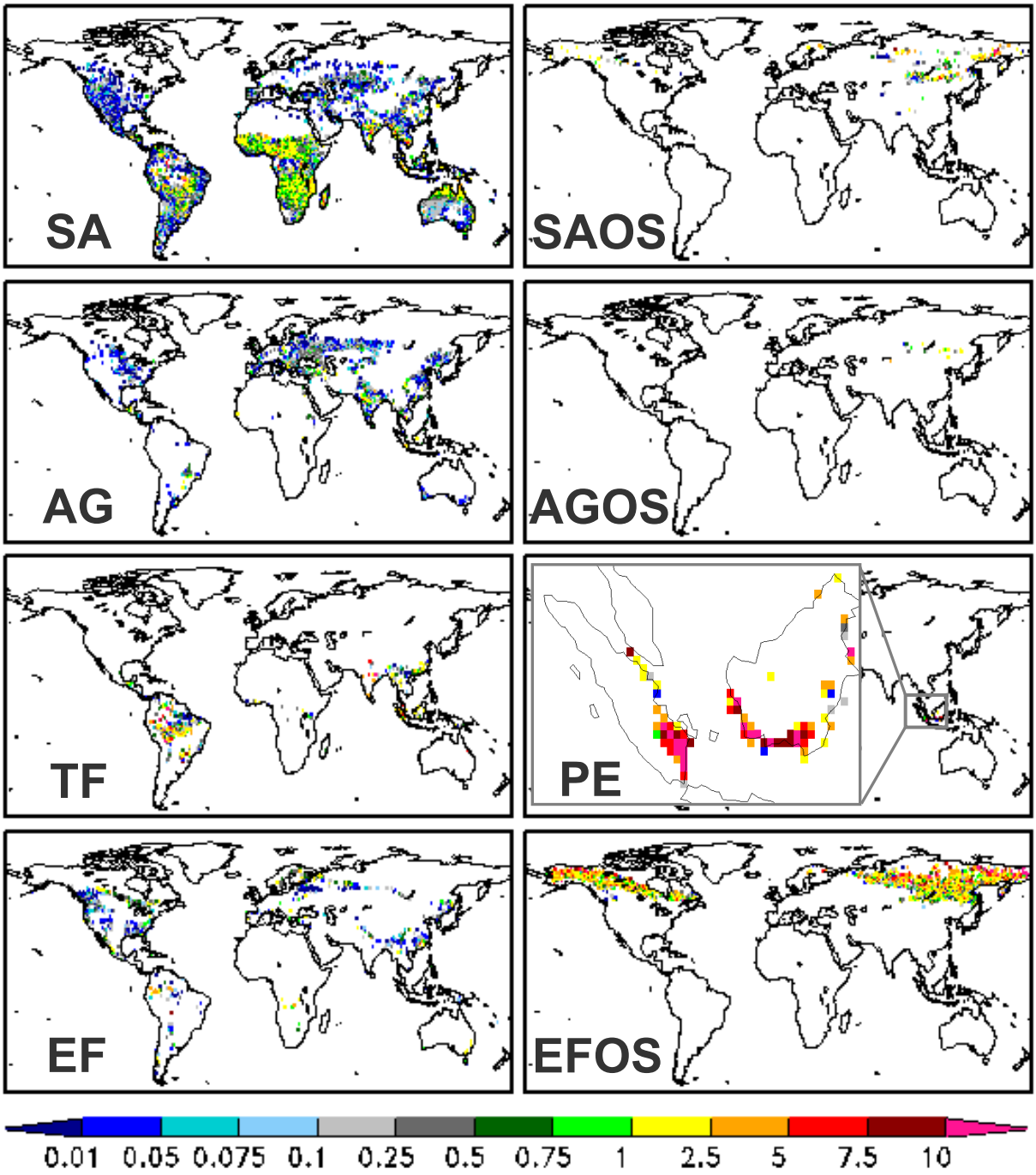

Figure 4-13: Spatial pattern of the slope (kg MJ-1) of the linear regression of monthly GFED3 DM with MODIS-FRP values. The regression was performed for each grid cell and stratified by fuel type (see description in Figure 4-3). The slope should theoretically be close to the conversion factor (CF) of 0.368 kg MJ-1 defined by Wooster et al. (2005).

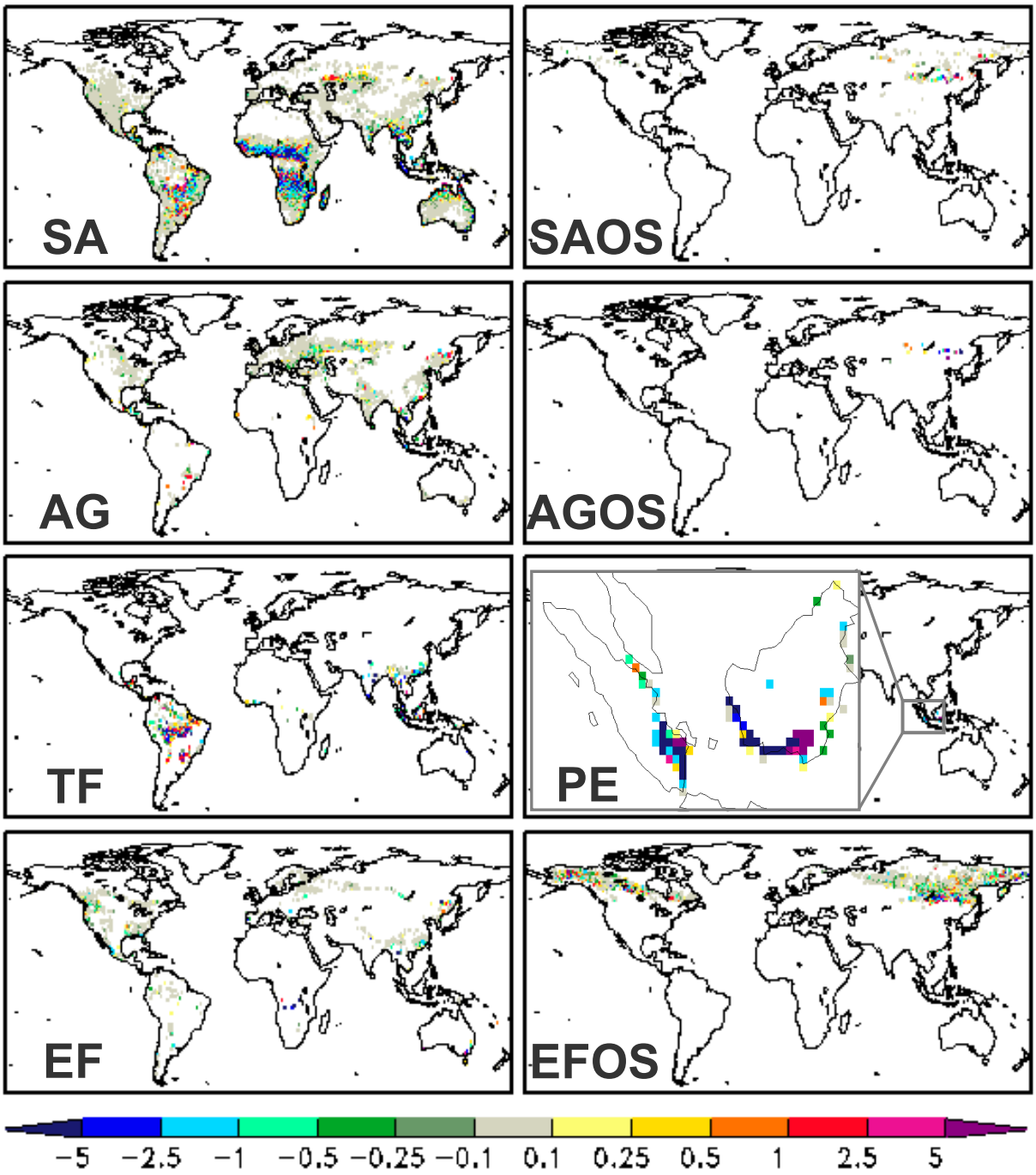

Figure 4-14: Spatial pattern of the intercept (in g DM month^{-1}) of the linear regression of monthly GFED3 DM with MODIS-FRP value, stratified by fuel type (see description in Figure 4-3).

In addition, the spatial pattern of the slope of the linear regression and the corresponding intercept is shown in Figure 4-13 and Figure 4-14. The intercept is close to zero (between -0.1 and 0.1 g DM month^{-1}) in most areas. A major exception can be observed in the equatorial African savanna region between around 20°S and 10°N: there are two meridional belts, one north of the Equator and the other south of around 10°S, where the intercept is below 1 g DM month^{-1} , and another meridional belt between the Equator and 10°S, where the intercept is above 1 g DM month^{-1} . The spatial pattern of

the intercept explains differences between the spatial features of the effective conversion factor (CF) (Figure 4-14) and those of the GFED3 to MODIS-FRP dry matter burned ratios (Figure 4-3) discussed above. Some of the spatial differences within a predominant fuel class might be explained by the differing fractional contribution of various vegetation types within a grid cell. This will be addressed in further studies.

5 GFASv0 vs. GFED3 (Carbon Monoxide)

5.1 Spatial Patterns

In Figure 5-1 annual total fire CO emissions estimates for the year 2009 are shown for both GFAS_v0 (section 2.2) and GFED3 (section 2.1). Because GFAS was scaled to GFED2, which had somewhat higher emissions than GFED3, and because the resolutions differ, no exact match is expected.

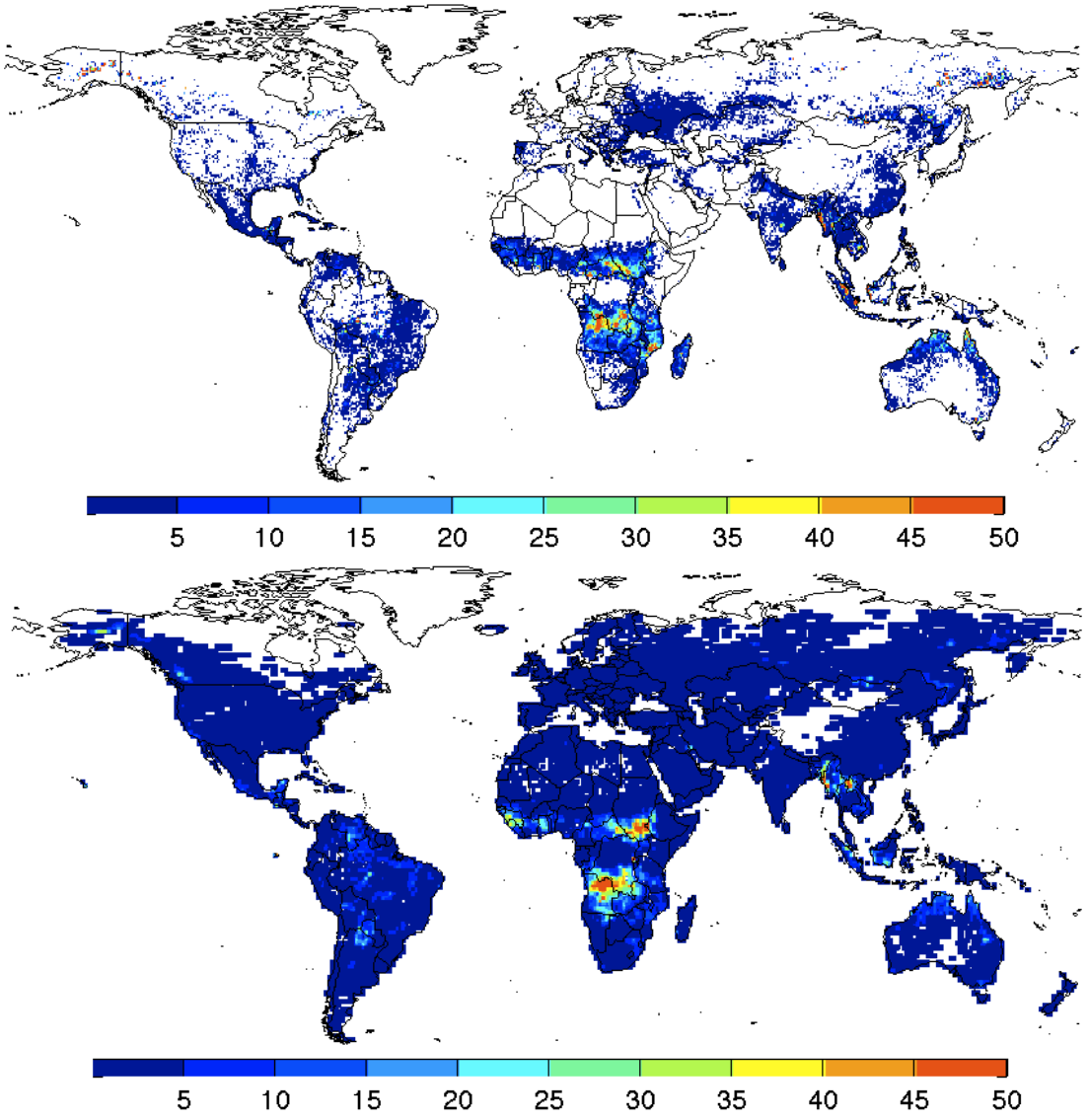

Figure 5-1: Annual total CO emissions (g CO m-2 year^{-1}) for GFED3 (top) and GFASv0 (bottom).

While in general the main burning regions match reasonably, differences are substantial. Most apparent is the much larger area where fires are observed in GFAS than in GFED, even though emissions are small in these areas. Besides due to the coarser resolution in GFASv0 (~125 km) compared to GFED3 (~50 km at the equator and finer at higher latitudes), this could have several reasons that are more extensively discussed in section 4.2 but can be summarized as:

- In GFED, a fire should burn a substantial fraction the 500m grid cell to be detected by the burned area algorithm. For GFAS, the FRP it is based on is capable of detecting much smaller fires. The MODIS instrument with its 1 km spatial resolution could, in favourable conditions, detect flaming fires of ~ 100 m^2 (0.01% of the grid cell) or possibly smaller.
- Hot point sources (gas flares, volcanoes) are detected by FRP but do not leave burned area signal. These could be removed with a static mask.
- Misinterpretation of the QA information of the FRP products.

Other apparent inconsistencies include 1) peat-burning regions in Indonesia where GFED assumes burning of peatlands, which may not be as readily detected by FRP – for example due to burning under the surface and also the overlying thick vegetation canopy in some areas, 2) the burning "hot spot" in northern Africa is in CAR according to GFED, but in southern Sudan according to FRP, 3) fires in eastern Siberia are of much higher intensity emissions-wise in GFED compared to FRP.

These discrepancies are most likely related to the different detection capabilities outlined above and require further investigation, with a strong focus on the reasons behind the spatial variability of the FRP over GFED slope (see section 4.2). It is encouraging that correlations between the 12 months of overlap between GFAS and GFED3 for each grid cell are high. This indicates again that even though FRP and GFED disagree to a large extent spatially, the temporal variability is very similar. The negative correlation in the Amazon basin coincides with the edge of the SEVIRI disk and requires further investigation.

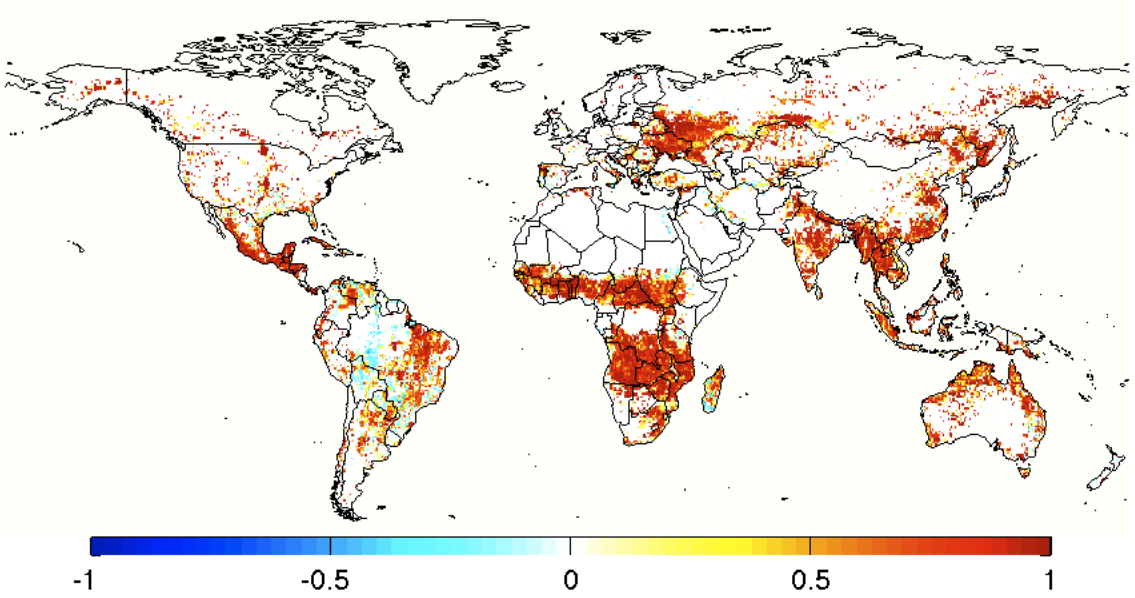

Figure 5-2: Correlation (r) between 12 monthly GFAS and GFED observations.

5.2 MODIS FRP vs. SEVIRI FRP

The differences between the MODIS and SEVIRI FRP products are further highlighted in Figure 5-3 and Figure 5-4. The former shows the average FRP density of 2009 calculated by the GFAS with input only from MODIS on the one hand and with input only from SEVIRI on the other hand. At the edges of the SEVIRI disk, FRP values are generally lower than the MODIS observations; see Eastern Europe, Madagascar & Argentina. This is behaviour may arise from an increased detection threshold of FRP observations for the large view zenith angles experienced by SEVIRI at these locations. The equatorial region of the upper Amazon is an exception, with widespread fire detections by SEVIRI where MODIS hardly sees any fires. In this region the GFASv0 and GFED3 emissions of CO are also anti-correlated, see above. Therefore, SEVIRI FRP product is probably particularly inaccurate and biased in this region. The main fire regions in Africa have different relative strengths. Further investigations are needed to determine whether this is caused by incomplete sampling of the diurnal cycle by MODIS or other effects.

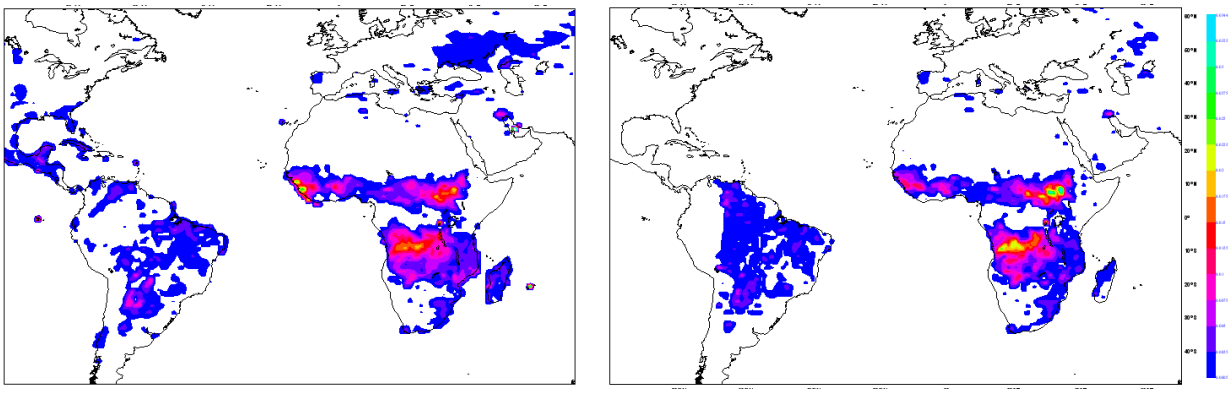

Figure 5-3: Average FRP density [W m^{-2}] registered in GFAS from the MODIS instruments (left) and SEVIRI (right) NRT product streams in 2009.

The time series of FRP observations by MODIS and SEVIRI in Figure 5-4 display the same fire seasons in Africa. However, clear differences remain: The maximum of the fire season in SH Africa observed by SEVIRI occurs one month earlier than the one in the MODIS observations. Conversely, the maximum of the NH African fire season seems to be shifted backwards in the SEVIRI data. Additionally, the MODIS data suggest that the fire activity in NH Africa stretches into April with about half its maximal strength/combustion rate, while SEVIRI data display a weaker tail. Finally, SEVIRI consistently records more burning between the fire seasons than MODIS. The reasons for these differences are not entirely clear. The main differences in the observations are:

- SEVIRI is resolving the diurnal cycle, while MODIS observations sample the fires more sparsely.
- SEVIRI's larger observations frequency also reduces the number and size of the observation gaps in the daily data.
- SEVIRI's higher detection threshold of 50MW, compared to 10MW for MODIS, is corrected in GFASv0 with a global correction factor of 2. This approximation neglects the variability of the fire size distribution with season, local time and location.

In Europe, the SEVIRI data completely misses fire events in April. These are the, presumably agricultural, burns in Eastern Europe that are also missing in Figure 5-3 and their omission can be explained by the degrading detection capabilities near the edge of the SEVIRI disk.

The Central America fire season around April is missing because it is completely outside the area observed by SEVIRI. The South American fire season around September and October, however, is not observed by SEVIRI even though much of the burning regions lie within the SEVIRI disk (albeit at high view zenith angles). Instead, fires are recorded throughout the year. This appears to be an error in the SEVIRI FRP data. The merged FRP product is dominated by the SEVIRI FRP observations because of their high observation frequency.

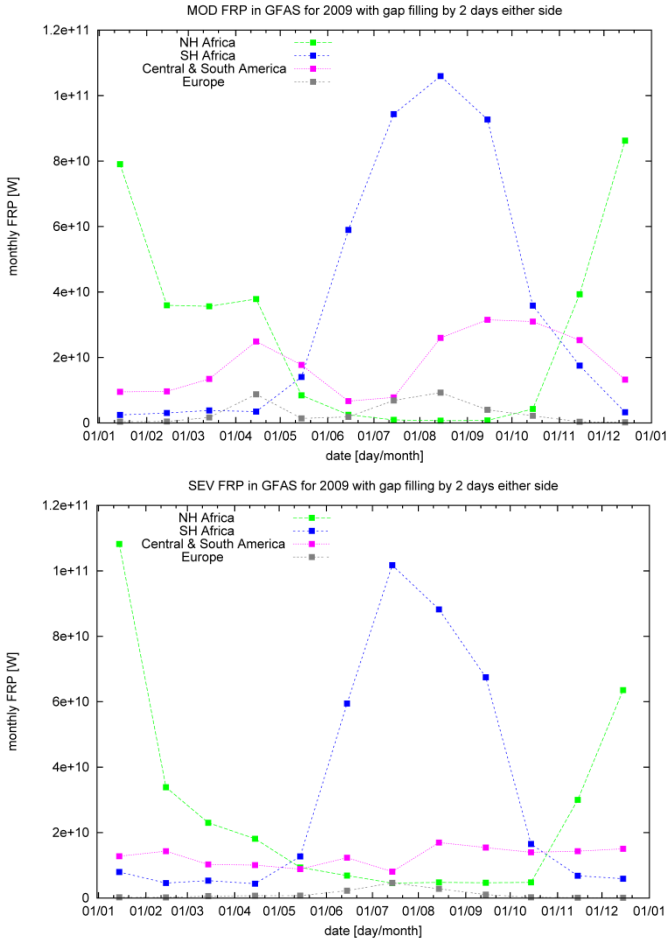

Figure 5-4: Monthly FRP estimates from MODIS (top) and SEVIRI (bottom) in the GFASv0 processing step 5. Note that SEVIRI observes only parts of the regions 'Central & South America' and 'Europe'.

5.3 Temporal Patterns

While the grid cell specific temporal correlation is high (Figure 5-2), this is not necessarily the case over larger regions (Figure 5-5). Part of this could be due to having one single scalar; while GFAS matches GFED2 on a global scale, regionally variations are explained by a relatively large number of small fires (e.g., Europe) or gas flares (e.g., the Middle East) that are detected by FRP but less likely by GFED, and the inclusion of organic soil (matter) burning that gives more weight to GFED (e.g., the boreal regions and Indonesia).), see Section 4.

Probably the largest temporal discrepancy occurs in South America, where GFASv0 (and thus FRP) maintains a relatively high baseline outside the fire season. While this could be due to GFED missing small fires that burn during the wet season, it seems unlikely that these fires lead to emissions about half of the peak fire season activity. Some of this discrepancy could by due to the data anomalies of SEVIRI (see section 5.2). FRP observations will overestimate substantially due to a large number of false detections. It has also been shown that in some cases, fires can be better detected in tropical forest with hotspots than with burned area. Further data analysis has to be carried out to elucidate the reasons for the observed discrepancies.

In most other important biomass burning areas, fire activity during the wet season (or winter season in boreal and temperate regions) is much further reduced than in South America according to both approaches. In addition, MODIS active fire data (blue line inFigure 5-5) also indicate much lower fire activity during the wet season in South America.

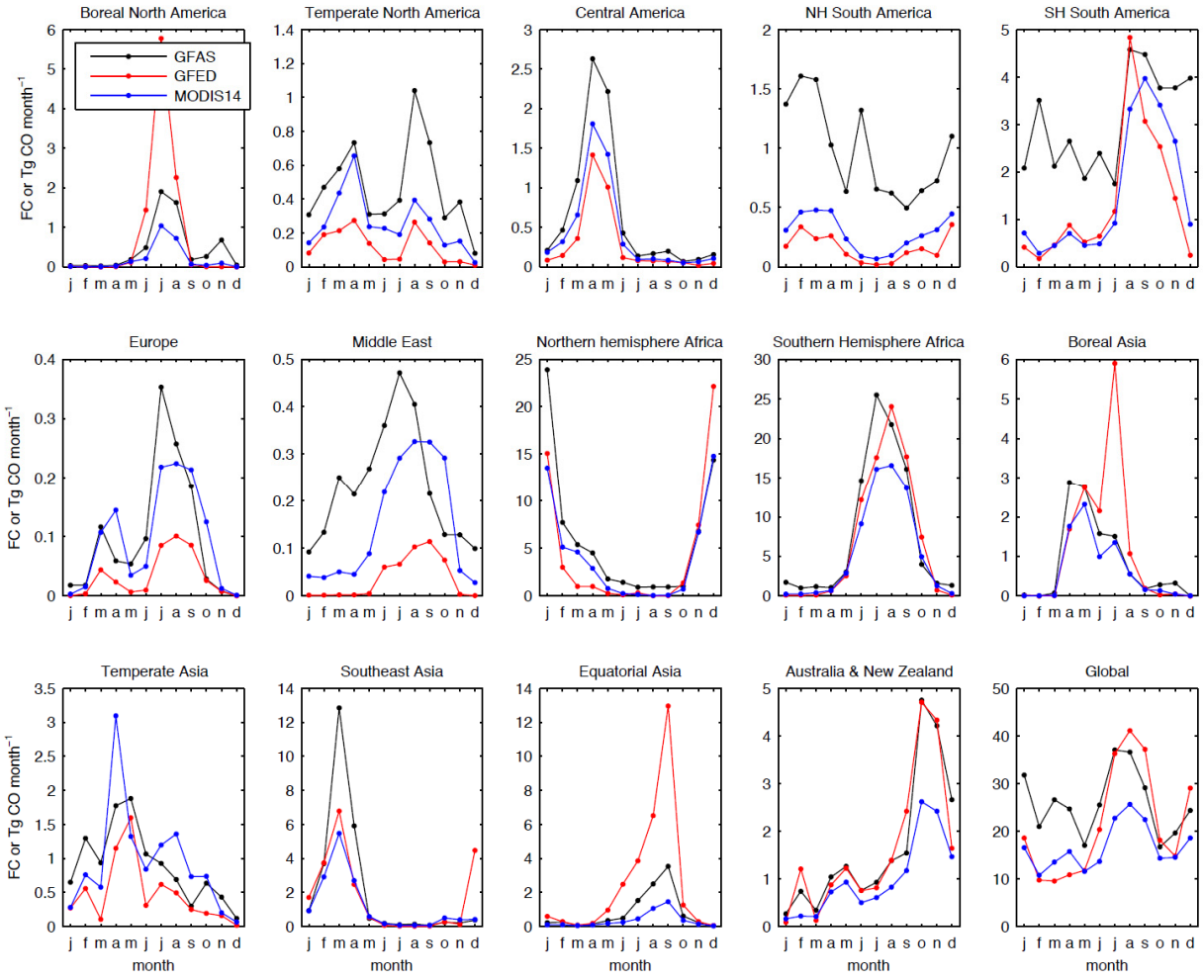

Figure 5-5: Monthly CO emissions estimates (Tg CO month^{-1}) for GFASv0 and GFED3, and MODIS (both Terra and Aqua) hotspots for 14 different basis regions, as well as the total global. Note that the number of MODIS hotspots was divided by 20.000 to arrive at similar scales.

Some information on the South American anomaly may come from inspecting the number of times a fire was observed in a grid cell during 2009 (Figure 5-6). Due to the larger footprint (125km), this number is expected to be higher for GFAS than for GFED. However, GFAS reports fires throughout the season in more or less all grid cells in the tropics, especially in the SEVIRI footprint. In contrast, MODIS active fires do not detect fires, or only in one or two months, in the interior of the Amazon, cf. *Fig.5-3*. Further scrutinizing the merging of SEVIRI and MODIS derived FRP (especially at the edge of the SEVIRI disk, see section 5.2) may shed light on the South America anomaly that is likely caused by the large-scale detection of relatively small fires outside the burning season.

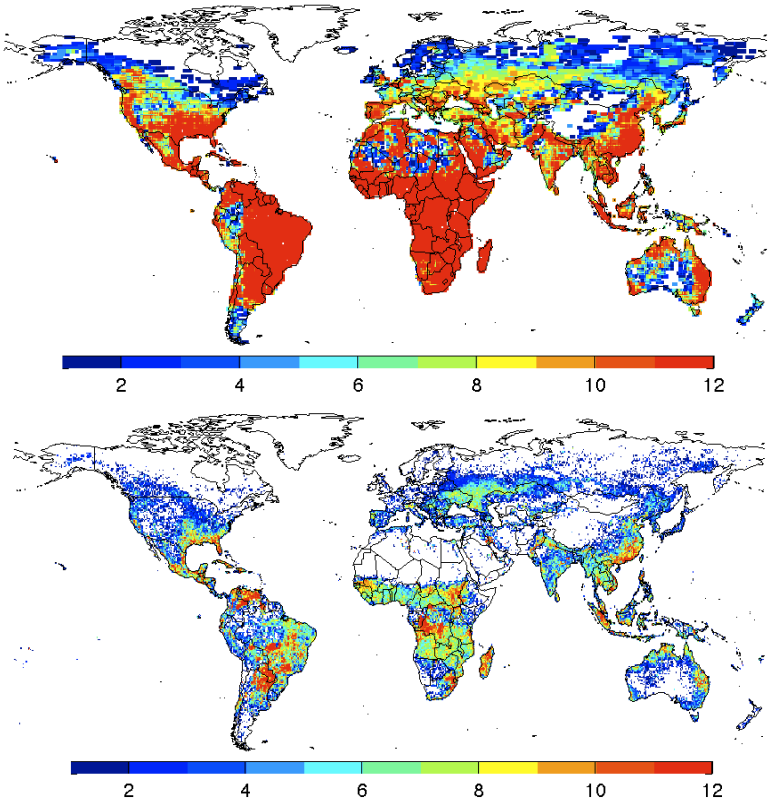

Figure 5-6: Number of months in 2009 with fire observations for MODIS hotspots (top, both Aqua and Terra) and GFAS (bottom).

One additional concern is the mismatch of peak fire season in southern Africa; where GFED peaks a month later than GFAS. Southern Africa is one of the most important biomass burning regions and comparing GFED with atmospheric measurements has highlighted that GFED peaks one or two months earlier than seen in aerosol optical depth or carbon monoxide. (e.g., Petron et al., 2004). The mismatch with GFAS would thus be even larger.

Currently, the GFASv0 calculates dry matter emissions with a global conversion factor from FRP. It will ultimately be able to distribute fire emissions in a higher spatial and temporal resolution than possible in GFED. A dominant land cover type (with regard to carbon emissions) based on GFED2 and literature-derived emission factors (EFs, Andreae & Merlet, 2001) are then used to calculate emissions of trace gases and aerosols. These EFs vary by about a factor 2-3 for different biome types within general easily oxidized fuels such as grasses burning more efficiently (more CO_2, less reduced gases) than coarse or wet fuels. In GFASv0 each grid cell was assigned a single land cover type class

based on GFED2. Emission factors were then applied based on this land cover type class (savanna, tropical forest, other forest). In GFED3, however, the fire type assignment is more dynamic with both changes over time and sub-grid cell partitioning. Specifically, within each grid cell and month the contribution of the fire types is calculated, and emission factors are applied to the fractional contributions. An example is shown in Figure 5-7 for Southern Africa where the contribution of woodland emissions changes over the course of the fire season in GFED (left graph). Based on a single woodland contribution scalar (dashed line in Figure 5-7 right-hand panel) the contribution of woodland burning is overestimated in the beginning of the season and underestimated in the peak fire season. Since woodland fires were assigned a different emission factor than the other main source in southern Africa (savanna and grassland fires), this would translate into overestimating reduced gas emissions (such as carbon monoxide) at the beginning of the season.

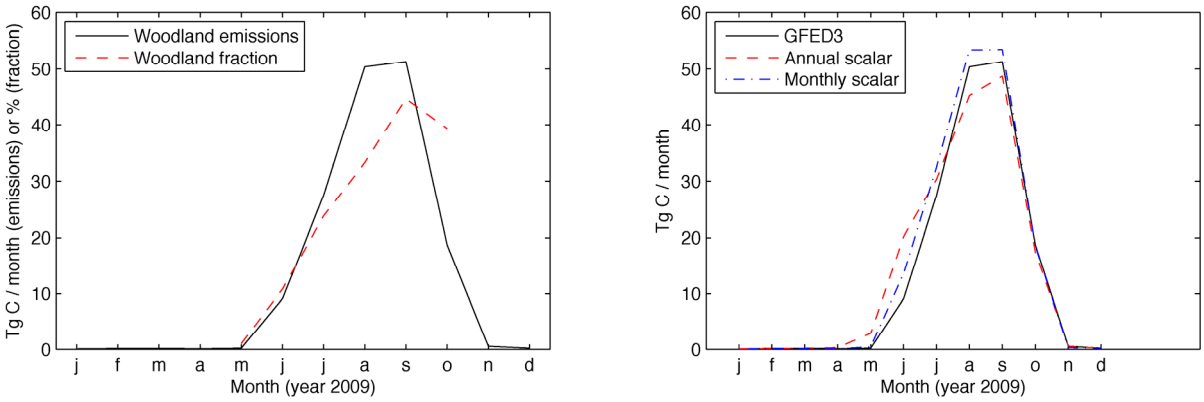

Figure 5-7: Seasonality of woodland carbon emissions and its fraction of total carbon emissions (left) and GFED3 woodland emissions as well as GFED3 woodland emissions based on total emissions combined with an annual scalar representing the amount of woodland burning, or a seasonal scalar. Scalars were averaged based on 2001-2008 data.

Part of the discrepancy could be resolved by introducing monthly scalars. The dashed blue line in Fig. 5-7 is based on the monthly woodland contribution climatology based on 2001-2008 data, and applied to 2009. While the absolute emissions are overestimated compared to GFED emissions (likely due to below-average woodland burning in 2009 compared to earlier years), the seasonal cycle is much better represented, translating into trace gas emissions which better resemble GFED emissions.

In the future, the conversion of dry matter burned to the various species emitted in GFAS should therefore be driven by monthly climatologies of the contribution of each fire type or even attempt to derive such information from the FRP data. Two additional potential sources of errors are:

1) GFED contributions are calculated monthly; this leads to substantial changes in emission factors applied to daily FRP values when moving from the final day of one month to the first day of the next month. This could be partly resolved by smoothing the monthly climatologies to daily values using spline fits. Potentially, also daily meteorological data and the observed FRP distribution with in global grid cells could be included to better apply emission factors. In a related project ("Emission factor modelling, the forgotten step in estimating fire emissions", funded by the Dutch Space Research Institute) MSc. Student T.T. van Leeuwen working at VU University Amsterdam with G.R. van der Werf is working to better address relations between climate, fire type, and emission factors. In the future, potential outcomes could be built into the GFAS framework.

2) In the tropics, the fire season is well defined and each year the same pattern of fire type seasonality and emission factors is more or less repeated – although some variations may occur in major El Nino years. In temperate and boreal regions, however, climatological conditions are more variable between years and the use of a climatology may not yield realistic conditions for a particular year. In addition, fires are not as widespread and climatologies will be based on fewer observations with possibly the need for geographical weighted regression approaches or usage of the above mentioned daily meteorological data and the observed FRP distribution with in global grid cells.

6 Agricultural Waste Burning

Agricultural waste burning (AGW), or the burning of crop residuals in the field, is a main source of air pollution in several regions (Figure 6-1). Within the MACC project, both D-FIRE and D-EMIS report AGW estimates so there is a risk of double counting. These estimates, however, are based on different methodologies and could be used to complement each other. While the D-FIRE based AGW emissions are calculated based on satellite data, D-EMIS AGW emissions area based on country-level reporting (possibly aided by satellite data).

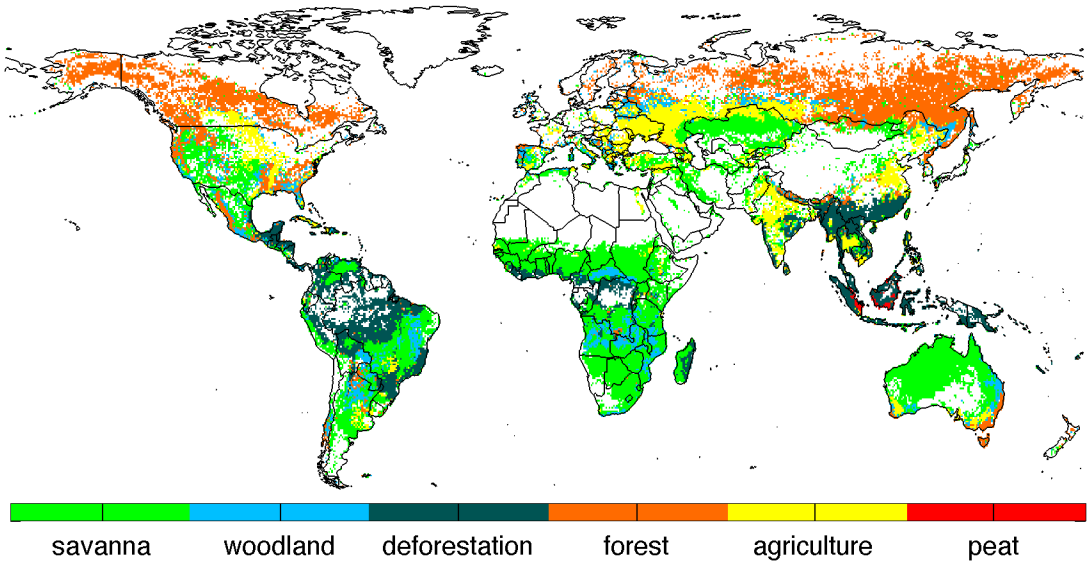

Figure 6-1: Dominant source of emissions according to GFED. The yellow areas indicate where AGW fires are the most important source of emissions.

AGW fires are in general small, and the fire signal may not be large enough to be detected by the algorithm used to detect burned area in 500-meter pixels as used in GFED (and which is the bases for the D-FIRE emissions). Some indirect evidence that this is indeed is the case comes from comparing GFED AGW estimates with those derived independently. The former is about 50 Tg C / year (global annual average) while for example Yevich and Logan (2003) estimated emissions of 200 Tg C / year. A similar value is derived when multiplying global total fire carbon emissions (2 Pg C / year) with the fraction of active fire detections that are observed in AGW areas (10%, Korontzi et al., 2003). These active fires have a much lower detection threshold than burned area estimates, and partly integrate the effect of burned area and fuel consumption.

For Europe, the D-FIRE and D-EMIS subgroups have compared the two approaches on country-level scale based on GFED vs. GAINS and EUCAARI estimates. The latter two are based AGW burning

and activity-specific emission factor (e.g. NOx, PM2.5 etc). GAINS is the IIASA model. EUCAARI is a TNO inventory for EU FP6 project EUCAARI but it relies for an important part on activity data obtained through collaboration with GAINS / IIASA. There are differences but the approach is certainly not independent.

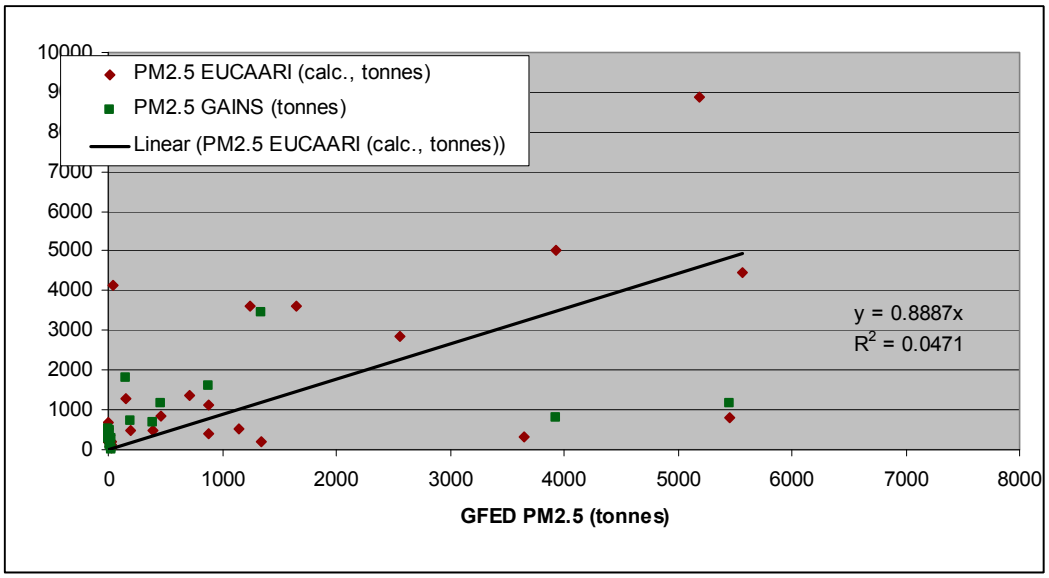

Figure 6-2: Comparison of PM2.5 data (all countries, except Russia and Ukraine).

In Figure 6-2 the comparison for PM2.5 emissions from both approaches is shown for the European domain. Russia and the Ukraine were excluded in the graph because EUCAARI and GAINS only include the European part of Russia whereas GFED covers the entire Russian domain. The comparison highlights the large differences, but also indicates that for several countries, GFED-based estimates exceed the ones reported by countries. This is unexpected and could be due to underreporting, possibly motivated by a ban imposed on AGW burning in Europe.

AGW emissions account for ~2% of total emissions in most European countries. From that perspective, double counting may not be dramatic, especially if country-level reporting may underestimate emissions. However, the strong seasonality of AGW fires and potential close proximity to urban centers will impact air quality more than the average annual contribution implies. For this reason, we aim to go into more detail regarding the comparison, with several possible steps:

1) Include non-European countries and more datasets (e.g., the IPCC emissions). Comparing to the AGW emissions calculated from MODIS FRP with the global FRP-DM conversion factor determined in this report may also shed light on the relative distribution of AGW between countries.

2) Merge the different approaches, potentially following these steps:

    a. Since GFED estimates are likely a lower bound, replace all country-level estimates if they are below GFED

    b. Apply the temporal and spatial distribution of GFED AGW emissions to country-level emissions, which usually are not distributed in space and time

3) Verify whether differences in country-level AGW emissions are due to different emission factors

7 Atmospheric Composition Forecasts based on GFASv0

MACC is providing a real time service that forecasts CO plumes from, amongst other sources, biomass burning and provides them to scientific campaigns. So far, there are no quantitative comparisons to observations. Qualitative comparisons with other smoke plume forecasting systems for the US indicate that the GFAS emissions are, however, correctly timed and placed (Kaiser et al. 2009a).

A study with the MACC NRT forecasting system for aerosols using either GFED2 emissions from 2003 or the GFASv0 aerosol emissions has been undertaken. The atmospheric aerosol forecasts are initialised from the analysis, which assimilates MODIS AOD observations, and run for four days with different fire emissions. The resulting aerosol optical depth (AOD) is compared to the one observed by AERONET stations. The bias and root mean square error of the AOD forecasts with respect to a global distribution of AERONET validation sites are shown in Figure 7-1. Both forecasts compare virtually identically to AERONET. The reason is that the MODIS AOD assimilation draws both model runs towards the truth. Also, the main biomass burning season produce smoke plumes that are to a large extent similar on a global scale in every year. Thus use of either of the fire emission data sets seems justified in an application that aims to represent the global-scale smoke abundance.

Figure 7-2 shows comparisons of the two AOD forecasts at two individual AERONET locations. At both locations the forecasts based on GFED2 of 2003 display plumes that are missing in the AERONET and MODIS observations (of 2009). The forecasts based on GFASv0, which is produced in real time, are superior in that they do not lead to misplaced plumes. Correct timing and location is obviously a crucial advantage for air quality forecasting. GFED emission of 2009 would also be expected to be superior in this respect, but the data are not available in real time.

The study shows that critical aspects of the accuracy of fire emission data sets manifest themselves at grid cell or regional resolutions. The global AERONET network is still too sparse to accurately assess these aspects. The satellite observations used for assimilation in the global MACC system offer an alternative with much better observational coverage for AOD, and additionally CO and other gases. Therefore, they should be used to further assess the GFAS emission products and calibrate any newly introduced parameters. In order to avoid interference from the data assimilation itself, experiments need to be set up as “passive assimilation”, which produces departure statistics without modifying the atmospheric fields. Such model simulations are planned for the second MACC phase.

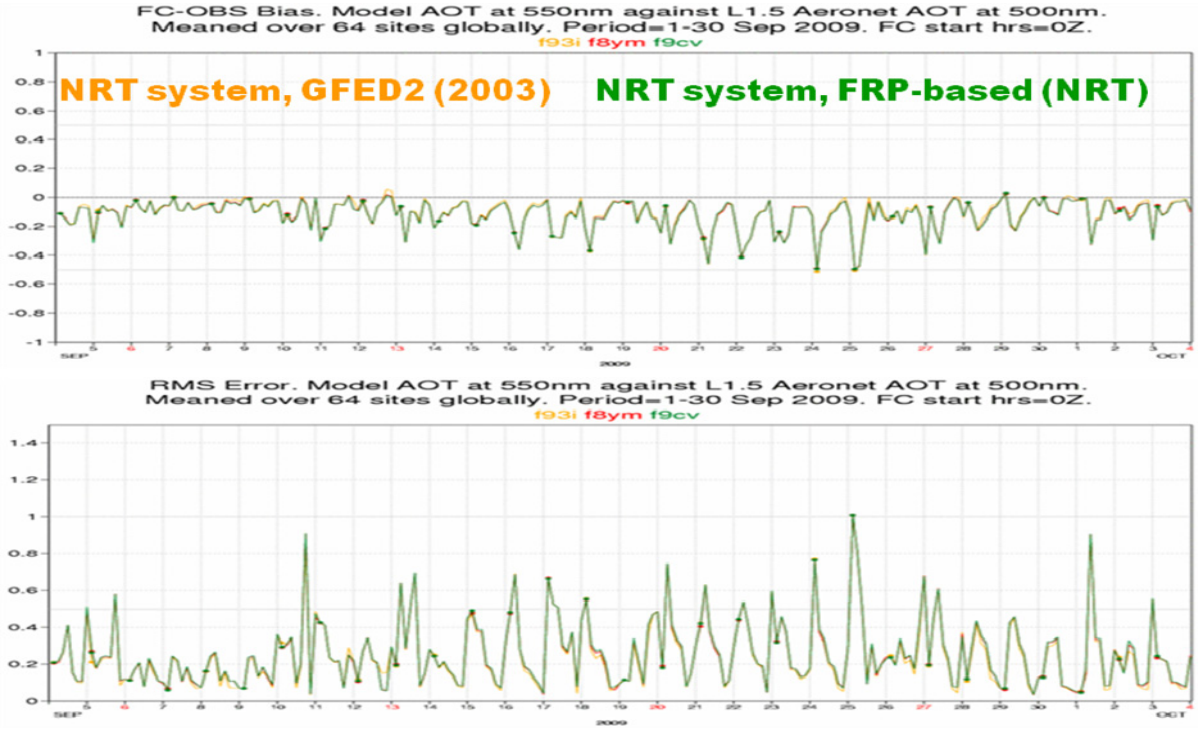

Figure 7-1: AOD Bias (top) and RMS error (bottom) of the MACC NRT aerosol forecasts with respect to 64 globally distributed AERONET stations. The forecasts based on GFED3 emissions of 2003 are plotted in yellow, those based on GFASv0 are plotted in green.

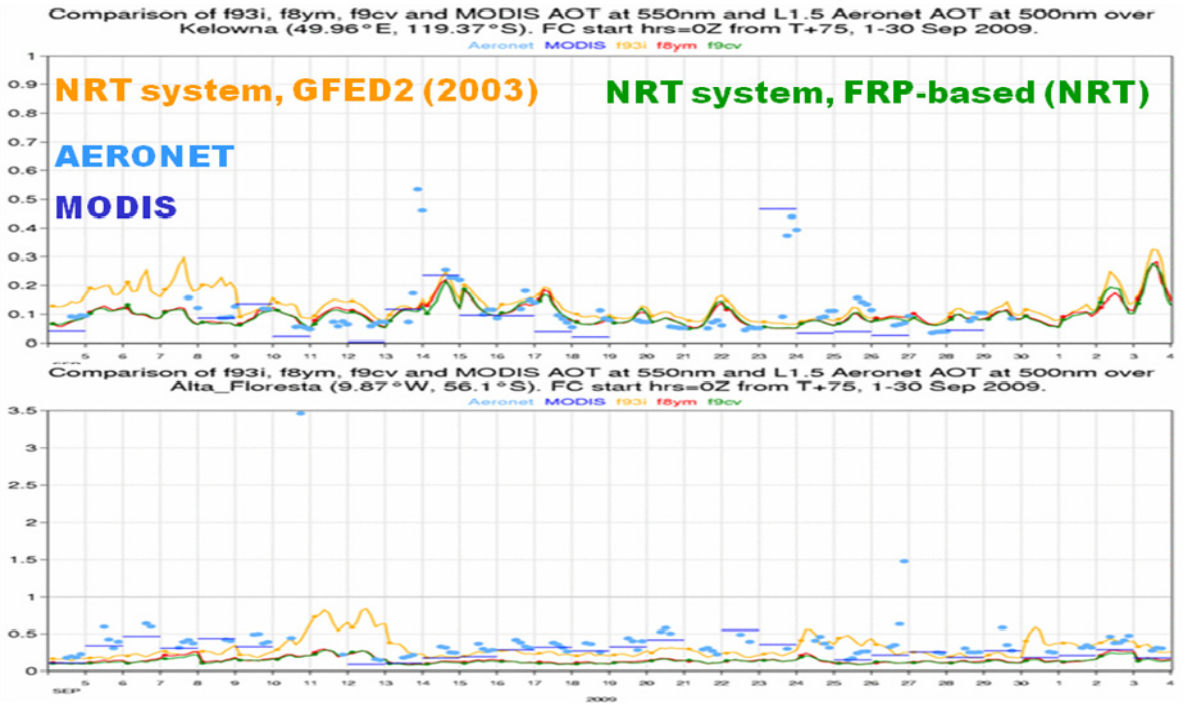

Figure 7-2: AOD time series of the MACC NRT aerosol forecasts compared to two selected AERONET stations and daily MODIS AOD. The forecasts based on GFED3 emissions of 2003 are plotted in yellow, those based on GFASv0 are plotted in green.

8 Recommendations for the Further Development of GFAS

We have compared a time series FRP fields calculated with a modified version of GFAS from MODIS FRP observations and GFASv0 real time emission products to GFED3 combustion rate and emission fields. For the purpose of this report, GFED3 serves as reference since it is an update of the scientifically most established fire emission inventory, GFED2. The comparisons show that:

1. Global combustion rate estimation from FRP observation is possible with conversion factors that are land cover specific or fuel load dependent. Such an approach will most likely yield combustions rates that are consistent with GFED3 within its expected accuracy (except for the number of observed fires discussed in the next bullet).
2. FRP observations exhibit more number of fire observations in each grid cell (N_{FIRE}) than GFED3. This leads to a reduction of the amplitude of seasonal fire variability. It may be caused by increased detection sensitivity of the FRP observations but further investigations are needed.
3. The GFASv0 emissions are already suitable as input for global atmospheric simulations with the exception of an anomaly over South America that is caused by the SEVIRI FRP product.

GFASv0 was set up with the primary objective of delivering correct spatial distributions and timings of the global biomass burning emissions in real time, to complements the capabilities of the atmospheric data assimilation systems in MACC. These systems are capable of adjusting aerosol and trace gas concentrations in the plume but require a priori information on the plume locations, including altitude, and relative mix of aerosol species. This study shows that the current GFAS set-up reasonably well reproduces and forecasts large-scale spatial and temporal fire emissions patterns, as well the emission strengths as estimated by GFED. How several improvements can be made to the framework in the near future:

1. The SEVIRI product over South America (towards the edge of the SEVIRI observation disk) seems to be unreliable. As soon as practically possible its use should be discontinued in the GFAS processing and replaced with GOES FRP data, which are expected to substantially improve the fire observations over the Americas. (Usage of the SEVIRI product over South America has already been disabled in the real time production GFASv0 on 17 June 2010. It will rely solely on MODIS in this area until GOES FRP observations are being merged.)
2. Instead of a single factor converting FRP to DM burned, GFAS should use land cover specific factors distinguishing SA, AG, TF, EF (no organic soil), EF(organic soil) and PE. The values derived from the presented comparison to GFED3 should be used (see Table 4-1).This recommendation establishes a compatibility of the burned DM estimation of GFED and GFAS that allows use of identical methodologies for the subsequent species emission calculation.
3. The translation from dry matter fire emissions to trace gas and aerosol emissions is based in GFASv0 on a static map with just four different land cover types. Thus the main source is unique for each grid cell. In GFED3, however, each grid cell resembles a mixture of fire types that also changes over time. GFAS should introduce monthly climatologies of these fire types and average the corresponding emission factors correspondingly to better resemble GFED3.
4. MACC should investigate whether a better mixture of emission factors may be achieved based on the meteorological conditions and FRP observations.

5. Gas flaring which is readily detected by the FRP products is a potential problem; detection of gas flares leads to emissions during times or regions where in reality no vegetation burns, and at the same time lowers fire emissions when fires actually do burn because emissions are scaled by total observed FRP (some of which may come from gas flaring). The GFAS should separate observed FRP into vegetation fires and gas flares, and exclude the latter from its analyses. Several thresholds are useful for this, for example temperature (vegetation fires normally do not burn when temperatures are below zero but gas flaring [e.g., in western Canada] continues), annual precipitation (to exclude desert areas where vegetation is not existent but where gas flaring is frequent), and the number of days in a year when FRP is observed (the larger the number the more likely this stems from a stationary source, seeFigure 4-5. The global gridded inventory on natural gas flaring established recently by Elvidge et al. (2009) could serve as additional source of information for the identification of commission errors due to the inclusion of gas flares into GFAS.
6. More extensive filling in of observational gaps should be implemented in the real time stream.
7. The MODIS FRP observations used in the GFAS system do not have any atmospheric correction applied, unlike the SEVIRI FRP observations. This is relatively simple to apply and can be based on precipitable water data from ECMWF. It will increase the raw FRP observations by perhaps 10 to 20 %, with maximum impact in humid areas. This adjustment should be implemented and the FRP to DM conversion factors should be adjusted correspondingly.
8. Passive assimilation experiments should be set up to utilise the extensive coverage of satellite-based atmospheric composition observations and the power of the global atmospheric assimilation systems implemented in MACC for the calibration of the conversion and emission factors in the GFAS. It will also allow validation of the day-to-day variability in the GFAS fire emission products. This will require an adequate treatment of fire plume rise.

9 References

Arino, O., Rosaz, J. M., and Poloup, P.: The ATSR World Fire Atlas and a Synergy with POLDER Aerosol Products Proceedings of the International Workshop on the Applications of the ERS Along Track Scanning Radiometer, 8, 1999.

Ballhorn U., Siegert F., Mason M. and Limin, S.: Derivation of burn scar depths and estimation of carbon emissions with LIDAR in Indonesian peatlands. PNAS 106 (50):21213-21218, 2009.

Cochrane, M. A., Alencar, A., Schulze, M. D., Souza, C. M., Nepstad, D. C., Lefebvre, P., and Davidson, E. A.: Positive feedbacks in the fire dynamic of closed canopy tropical forests, Science, 284(5421), 1832– 1835, 1999.

Ellicott, E., Vermote, E., Giglio, L., and Roberts, G.: Estimating biomass consumed from fire using MODIS FRE, Geophys. Res. Lett., 36, 1-5, doi:10.1029/2009GL038581, 2009.

Elvidge, C.D., Ziskin, D., Baugh, K.E., Tuttle, B.T., Ghosh, T., Pack, D.W., Erwin, E.H., and Zhizhin, M. A: Fifteen Year Record of Global Natural Gas Flaring Derived from Satellite Data. Energies 2, 595-622, 2009.

Freeborn, P. H., Wooster, M. J., Hao, W. M., Ryan, C. A., Nordgren, B. L., Baker, S. P., and Ichoku, C.: Relationships between energy release, fuel mass loss, and trace gas and aerosol emissions during laboratory biomass fires, J. Geophys. Res., 113, D01301, doi:10.1029/2007JD008679, 2008.

Giglio, L., Csiszar, I., Restás, Á., Morisette, J. T., Schroeder, W., Morton, D., and Justice, C. O.: Active fire detection and characterization with the Advanced Spaceborne Thermal Emission and Reflection Radiometer (ASTER). Remote Sensing of Environment, 112, 3055-3063, 2008.

Giglio, L., Descloitres, J., Justice, C. O., and Kaufman, Y. J.: An enhanced contextual fire detection algorithm for MODIS, Remote. Sens. Environ., 87, 273-282, doi:10.1016/S0034-4257(03)00184-6, 2003.

Giglio, L., Kendall, J. D., and Mack, R.: A multi-year active fire dataset for the tropics derived from the TRMM VIRS, Int. J. Remote Sens., 24, 4505-4525, doi:10.1080/0143116031000070283, 2003b.

Giglio, L., Loboda, T., Roy, D. P., Quayle, B., and Justice, C. O.: An active-fire based burned area mapping algorithm for the MODIS sensor, Remote. Sens. Environ., 113, 408-420, doi:10.1016/j.rse.2008.10.006, 2009.

Giglio, L., Randerson, J. T., van der Werf, G. R., Kasibhatla, P. S., Collatz, G. J., Morton, D. C., and DeFries, R. S.: Assessing variability and long-term trends in burned area by merging multiple satellite fire products, Biogeosciences, 7, 1171-1186, 2010.

Giglio, L., van der Werf, G. R., Randerson, J. T., Collatz, G. J., and Kasibhatla, P. S.: Global estimation of burned area using MODIS active fire observations, Atmos. Chem. Phys., 6, 957-974, 2006.

Hui, D. F., and Jackson, R. B.: Geographical and interannual variability in biomass partitioning in grassland ecosystems: a synthesis of field data, New Phytologist, 169, 85-93, doi:10.1111/j.1469-8137.2005.01569.x, 2006.

Kaiser et al.: Global Real-time Fire Emission Estimates Based on Space-borne Fire Radiative Power Observations. AIP Conference Proceedings, 1100, 645–648, 2009b.

Kaiser et al.: The MACC Global Fire Assimilation System: First Emission Products (GFASv0). ECMWF Tech. Memo. 569, 2009a.

Kasischke, E. S., Hyer, E. J., Novelli, P. C., Bruhwiler, L. P., French, N. H. F., Sukhinin, A. I., Hewson, J. H., and Stocks, B. J.: Influences of boreal fire emissions on Northern Hemisphere atmospheric carbon and carbon monoxide, Global Biogeochem. Cycles, 19, GB1012, doi:10.1029/2004GB002300, 2005.

Parmar, R. S., Welling, M., Andreae, M. O., and Helas, G.: Water vapor release from biomass combustion, Atmos. Chem. Phys., 8, 6147-6153, doi:10.5194/acp-8-6147-2008, 2008.

Pereira, G., Freitas, S.R., Moraes, E.C., Ferreira, N.J., Shimabukuro, Y.E., Rao, V.B., and Longo, K.M.: Estimating trace gas and aerosol emissions over South America: Relationship between fire radiative energy released and aerosol optical depth observations, Atmospheric Environment 43, 6388–6397, 2009.

Petron, G., Granier, C., Khattatov, B., Yudin, V., Lamarque, J. F., Emmons, L., Gille, J., and Edwards, D. P.: Monthly CO surface sources inventory based on the 2000– 2001 MOPITT satellite data, Geophys. Res. Lett., 31, L21107, doi:10.1029/2004GL020560, 2004.

Randerson, J. T., Thompson, M. V., Malmstrom, C. M., Field, C. B., and Fung, I. Y.: Substrate limitations for heterotrophs: Implications for models that estimate the seasonal cycle of atmospheric CO2, Glob. Biogeochem. Cy., 10, 585-602, 1996.

Roberts, G. J., and Wooster, M. J.: Fire detection and fire characterization over Africa using Meteosat SEVIRI, IEEE Trans. Geosci. Remote Sensing, 46, 1200-1218, doi:10.1109/TGRS.2008.915751, 2008.

Ruesch, A., and Gibbs, H. K.: New IPCC Tier-1 Global Biomass Carbon Map For the Year 2000. Available online from the Carbon Dioxide Information Analysis Center [http://cdiac.ornl.gov], Oak Ridge National Laboratory, Oak Ridge, Tennessee, 2008.

Ryan, K.C.: Dynamic interactions between forest structure and fi re behavior in boreal ecosystems. Silva Fennica 36(1): 13–39, 2002.

Schultz, M.: On the use of ATSR fire count data to estimate the seasonal and interannual variability of vegetation fire emissions, Atmos. Chem. Phys., 2, 387-395, 2002.

Seiler, W., and Crutzen, P. J.: Estimates of gross and net fluxes of carbon between the biosphere and atmosphere from biomass burning, Climatic Change, 2, 207-247, 1980.

Stocks, B. J. and Kauffman, J. B.: Biomass consumption and behavior of wildland fires in boreal, temperate, and tropical ecosystems: Parameters necessary to interpret historic fire regimes and future fire scenarios, in: Sediment Records of Biomass Burning and Global Change, Clark, J. S. et al. (Eds.), Springer-Verlag, New York, 169-188, 1997.

ter Steege, H., Pitman, N. C. A., Phillips, O. L., Chave, J., Sabatier, D., Duque, A., Molino, J.-F., Prevost, M.-F., Spichiger, R., Castellanos, H., von Hildebrand, P., and Vasquez, R.: Continental-

scale patterns of canopy tree composition and function across Amazonia, Nature, 443, 444-447, doi:10.1038/nature05134, 2006.

Usup, A., Hashimoto, Y., Takahashi, H., and Hayasaka, H.: Combustion and thermal characteristics of peat fire in tropical peatland in Central Kalimantan, Indonesia. Tropics 14:1–19, 2004.

van der Werf, G. R., Randerson, J. T., Collatz, G. J., and Giglio, L.: Carbon emissions from fires in tropical and subtropical ecosystems, Global Change Biology, 9, 547-562, 2003.

van der Werf, G. R., Randerson, J. T., Giglio, L., Collatz, G. J., Kasibhatla, P. S., and Arellano, A. F.: Interannual variability in global biomass burning emissions from 1997 to 2004, Atmos. Chem. Phys., 6, 3423-3441, 2006.

van der Werf, G.R., Randerson, J.T. L. Giglio, L., Collatz, G. J., Mu, M., Kasibhatla, P. S., Morton, D. C., DeFries, R. S., Jin, Y, and van Leeuwen, T. T. : Global fire emissions and the contribution of deforestation, savanna, forest, agricultural, and peat fires (1997–2009), Atmos. Chem. Phys. Discuss., 10, 16153-16230, 2010.

Wooster, M.J and Zhang, Y.-H.: Boreal Forest Fires Burn Less Intensely in Russia than in North America. Geophys. Res. Lett. 31: doi:10.1029/2004GL020805O, 2004.

Yevich, R., and Logan, J. A.: An assessment of biofuel use and burning of agricultural waste in the developing world, Glob. Biogeochem. Cy., 17, 1095, doi:10.1029/2002GB001952, 2003.

Annex: History of the use of fire emissions in GEMS and MACC

GEMS/MACC SERVICE	Time period	Fire emission source	Fire emission resolutions
Aerosol, reactive & greenhouse gases (GEMS reanalysis)	Jan 2003 – Sep 2009	GFED2, 8-day resolution	8 days, 1 deg
aerosol, reactive & greenhouse gases (MACC reanalysis)	Jan 2003 – present	GFED3.0, redistributed with MODIS FRP	1 day, 0.1 deg
CO tracer forecast (NRT)	Jul 2008 – present	GFASv0	1 day, 125 km
Aerosol forecast (NRT)	Jul 2008 – Jan 2010	GFED2 (of 2003)	1 month, 1 deg
	Jan 2010 – Apr 2010	GFED2 (of 2004)	1 month, 1 deg
	Apr 2010 – present	GFASv0	1 day, 125 km
Aerosol, greenhouse gas forecast (delayed mode)	Jun 2009 – present	GFASv0	1 day, 125 km
Reactive gases (NRT)	Jul 2008 – present	GFED2	1 month, 1 deg